Climatic and cave setting influences on drip water fluorescent organic matter over an annual cycle in Northwestern Spain and implications for fluorescent laminations in stalagmites

Laura Sibylla Endres[1], Céline Jacquin[2],Saul González-Lemos[3], Laura Rodriquez-Rodriquez[3], Jakub Sliwinski[4], Nikita Kaushal[1], Oliver Kost[1] and Heather Marie Stoll[1]

[1]Geological Institute; ETH Zürich, Sonneggstrasse 5, 8092 Zürich, Switzerland

[2] EAWAG; CH-8600 Dübendorf, Switzerland

[3] Departamento de Geología; Universidad de Oviedo, Spain

[4] School of Earth and Environmental Sciences, University of St. Andrews; Queen's Terrace, St. Andrews KY16 9TS

Corresponding author: Laura Sibylla Endres (endres@erdw.ethz.ch, Phone: +41 (0)44 632 86 13)

ABSTRACT

Speleothem fluorescence may elucidate past vegetation dynamics, while microscale fluorescent laminations can provide annually resolved chronology. However, the origin of speleothem fluorescence and the mechanism responsible for the formation of micrometer scale fluorescent lamination in stalagmites, are not well constrained by monitoring studies. Here, we present results from a year-long monthly drip water monitoring from seven locations in La Vallina cave (Northwestern Spain). Fluorescence was quantified by excitation-emission matrices (EEM) spectrofluorometry. Five distinct components were resolved by parallel factor analysis (PARAFAC) modeling, including previously described humic-like, and protein-like components as well as an additional component suggesting a contribution of indigenous fluorescence sourced from the bedrock. Variations in the overlying vegetation and in the water reservoir age contribute to differences in the fluorescent components among different drip sites. While some active stalagmites feature annual to sub-annual fluorescent laminae, the drip water does not support higher abundance of humic-like fluorescence during the rainy season as a primary cause for layer formation. The constancy in humic-like fluorescence, likely to arise due to abiotic interactions with the bedrock, highlights possible other mechanisms on fluorescent layer formation, such as growth rate control over the dilation of the fluorescence signal in the stalagmite.

KEYWORDS

banding, speleothem, monitoring, karst aquifer, climate reconstruction, proxy development, PARAFAC, spectrofluorometer, absorbance, EEM

INTRODUCTION

Fluorescence is a common feature in speleothems from many caves and is generated by the dissolved organic matter (DOM) preserved in the speleothems. Speleothem fluorescence has been recognized for many decades (O'Brien, 1956) and has been characterized in organics dissolved from the stalagmite matrix (Pearson et al., 2020) as well as by surface scan in-situ analysis (Perrette et al., 2005). The in-situ distribution of fluorescence in stalagmites has been studied in thin or thick sections using UV excitation and detection on photographic film (Shopov et al., 1994) or detection of reflected fluorescence using epifluorescence microscopes (Baker et al., 1993; Luetscher et al., 2021), fibre-optics extensions connected to spectrofluorometer (McGarry and Baker, 2000), or on a polished section using a pulsed laser of a fixed wave length (Quiers et al., 2015) and confocal laser scanning microscopy (CLSM) ((Sliwinski and Stoll, 2021). From in-situ techniques, fine (5 to 1000 micron) scale alternations of high- and low fluorescence intensity perpendicular to the growth axis, have been described from many stalagmites from mid-latitude regions and this layering has been demonstrated to be annual in many cases (Baker et al., 2008; Proctor et al., 2000). The fluorescent layer intensity complexly interacts with speleothem trace element chemistry (Huang et al., 2001; Sliwinski et al., 2022). In such stalagmites, several authors have suggested the seasonal peak in fluorescence intensity is due to an increased in-flux of dissolved organic matter (DOM) in drip waters during increased autumn leaf litter and rainfall (Borsato et al., 2007; Kwiecien et al., 2022; McGarry and Baker, 2000), or alternately due to fine soil blown into the cave as an aerosol (Fairchild and Baker, 2012; Luetscher et al., 2021). In addition to changes in DOM input, changes in adsorption behavior at the crystal level, induced by variations in environmental and cave conditions such as pH, redox state and cave ventilation, could also cause variations in the incorporation of the fluorescent DOM ((Ramseyer et al., 1997; Sliwinski et al., 2022). Where the processes driving fluorescent layers can be demonstrated to be annual, then fluorescent banding can be exploited as a paleo-seasonality indicator (Ramseyer et al., 1997; Blyth et al., 2008; Sliwinski and Stoll, 2021; Orland et al., 2012) or to improve age models through fluorescent layer counting (Kwiecien et al., 2022). However, due to the limited number of monitoring studies and laboratory experiments available, direct evidence for fluorescent banding formation is sparse and the physical process is currently not understood in detail.

Speleothem and drip water organics originate from surface vegetation (e.g. lignin macromolecules), animal byproducts and soil processes; but also from biofilms and microbes living in the karst environment (McGarry and Baker, 2000; Fairchild and Baker, 2012). In the carbonate aquifer, organic matter can be degraded by microbial metabolism (Xia et al., 2022) or abiotically through adsorption on the bedrock. In lab experiments by Jin and Zimmermann (2010), DOM adsorption on carbonate host-rock was enhanced for high influx and long retention times. Adsorption in the same study acts similar to a ”buffer”, because organics covering the active crystal surfaces have been shown to inhibit bedrock leaching, and in contrast, low concentrations of DOM dissolved in water led to a release of indigenous organic matter from the host rock. Further lab speleothem growth experiments indicate that the presence of organic matter in the drip water can alter the fabric of the precipitated carbonates and precipitation kinetics (Pearson et al., 2020). The chemical structure of the organic matter also influences inorganic colloid coagulation (Wilkinson et al., 1997), and therefore the associated trace element transport through the aquifer and incorporation into the calcite matrix (Blyth et al., 2008), especially for first-row transition metals (Lindeman et al., 2021).

Only a minor part of the total DOM incorporated in speleothem fluoresces, often associated with aromatic ring structures(Aiken, 2014). Fluorescence occurs due to a three-step process: 1) a molecule is excited to a higher electronic state by absorption of a photon, 2) the molecule relaxes to lowest excited singlet state (vibrational relaxation) and 3) the molecule emits light to return to ground state (Lakowicz, 2006). The possible total fluorescence yield depends on molecular structure and is higher for more “rigid” structures, such as aromatic rings (Reynolds, 2014). Because fluorescence does not directly measure organic molecules, but rather the interaction of functional groups with photons, fluorescence does not provide a unique identification of the compounds present. Nonetheless, differing categories of fluorescent DOM are preferentially excited by, and emit, at different wavelength ranges (Coble et al., 2014). In the liquid phase, such as drip waters or dissolved carbonate, three-dimensional excitation-emission matrices (3D EEM) can be measured with modern spectrofluometers to provide characterization of the range of DOM types present and has been used extensively to study fresh and marine waters over the last decades. Two main categories of fluorescent DOM have been described: humic-like fluorescence, which resembles spectral features of isolated humic and fulvic acids (Alberts and Takács, 2004), and protein-like fluorescence, resembling fluorescence of amino acids such as trypophan and tyrosine (Coble et al., 2014). Humic-like fluorescence is characterized by the presence of a double peak in the EEMs and broader peaks, because it is thought to originate mostly from degradation of terrestrial biomaterial, which typically consists of molecules of higher molecular weight and encompasses a number of different compounds. Humic-like fluorescence also has been found to preferentially adsorb to the bedrock (Jin and Zimmerman, 2010). Protein-like, in contrast, consists of more isolated compounds with lower molecular weight and is thought to be more of microbial origin. Individual EEMs have been described by the main peaks in excitation-emission wavelength pairs based on literature, e.g. Coble peak nomenclature (Coble et al., 2014) or by ratios of the intensity at fixed excitation-emission wavelength pairs (e.g. the fluorescence index, McKnight et al. (2001)). More recently, parallel factor analysis (PARAFAC, Stedmon and Bro (2008)) has emerged to compile a model which describes the main fluorescent components and variability over an entire dataset. The generation of a PARAFAC model enables further discussion about the individual contributions to overall fluorescence and also allows to compare the dataset with other published models through the OpenFluor database (Murphy et al., 2014a).

Speleothems beaker precipitation experiments incorporate peat water DOM (Pearson et al., 2020). Prior studies of ground and cave drip waters have indicated dominant peaks in humic-like fluorescence, with seasonally variable peak wavelengths (Baker and Genty, 1999). Compared to overlying soil water fluorescence, spectra of drip water are likely to be blue-shifted, because of preferential adsorption on bedrock (Philibert et al., 2022; Jin and Zimmerman, 2010) and continued microbial degradation. Additionally, microbial fluorescence has been suggested to be important for cave waters (Birdwell and Engel, 2010). Microbial ("protein-like") fluorescence could occur in the cave system, but also be related to livestock above the karst (Mudarra et al., 2011). In one study comparing EEM spectra of three dissolved flowstone samples and the drip waters feeding them, the flowstones showed evidence of microbial peaks that are not seen in the drip waters feeding them (Pearson et al., 2020). PARAFAC modeling is common in water research and has been used briefly by Rutlidge (2014, 2015) to investigate DOM in drip waters after irrigation and also by Pearson et. al (2020).

In this present study, we have analyzed the evolution of fluorescent DOM in drip water at multiple drip sites within La Vallina cave in NW Spain to contribute to a better understanding of the spatial and temporal variations of organic matter in drip water and improve our understanding of stalagmite fluorescence signals. We characterize the components of drip water fluorescence using a PARAFAC model, and compare this model to cave properties, drip water chemistry and climatic influences. The analysis is extended through measurements of fluorescence in the dissolved bedrock and by CLSM images of actively growing stalagmites from the same cave. We evaluate the implications for inferring past changes in landscape and climatic processes from stalagmite fluorescence, and for the interpretation of annual to subannual fluorescence lamination in stalagmites.

STUDY SITE

Our study was conducted in La Vallina cave, situated near the town of Porrúa in Northwestern Spain (43°27’38’’N, 5°04’04 ‘’W, Fig.1). Under present-day conditions, the cave entrance is located 2.5 km from the coastline at an altitude of 70 m above the sea level. La Vallina formed within the carboniferous dark sulfidic massive micritic limestone of the Barcaliente formation. The bedding is subvertical, dipping 70° to the North. Barcaliente formation is rich in amorphous organic matter and classified as containing type II and III kerogen (Álvarez et al., 2019). Numerous block falls throughout the cave are consistent with a seismically active shallow crust (Delavaud et al., 2012). Karstification has led to several dolines, which can be recognized at the surface above the cave.

For this study, we selected seven locations within the cave system at which to monitor organics in drip water for one year from May 2020 – May 2021. Except for Mushroom (*MUS*), all sampling locations are positioned in the upper of two cave galleries. Vegetation and land area above the cave are significantly influenced by anthropogenic activities. A former primary deciduous forest has been largely exchanged with eucalyptus trees, which have been introduced in the region since the 19th century for wood production. The stem diameter of the current eucalyptus trees indicates ages around 60 years. Compared to other trees, eucalyptus has deep roots and a high water demand, which may have an effect on present-day cave hydrology. Furthermore, parts of the land have been exposed to fire activity and are currently covered with ferns. Exceptions are a few remaining oak trees close to the sampling location “Forest” (Fig.1). Other parts of the land above the cave are used as pasture for farm animals today. The detailed conditions for each sampling location are presented in Table 1 and Supplementary Table 1.

Present day regional climate, primarily controlled by the proximity to the North Atlantic ocean, is mild and warm. It can be classified as “Cfb” [temperate, with a warm summer, but no dry season], according to the Köppen-Geiger classification (Köppen, 1884; Peel et al., 2007). The closest weather station (Llanes, 4.2km NE of the cave, at the coast) has recorded a precipitation of 1267 mm/yr and an annual mean temperature of 15.3°C for the study period May 2020 - May 2021. The weather patterns over Northern Iberia are predominantly influenced by the westerlies with most incoming precipitation originating from Atlantic front systems and exhibit a long-term weighted annual mean $\delta^{18}O$ of -5.75 ± 0.34 ‰ (Santander GNIP station, 2000-2015, IAEA/WMO (2022)).

METHODS

Experimental Methods

Field Campaign

Drip water samples were collected from May 2020 to May 2021 on a quasi-monthly basis. Bi-weekly sampling was carried out in autumn to evaluate the impact of a higher amount of rain and falling leaves on drip water chemistry. Four locations (*GRA, GLO, SKY, PLA)* were monitored over the entire year, *FOR* was monitored from September 2020-May 2021, *MUS* and *SNO* only for three dates in 2021.

From each location, samples for fluorescence measurements have been collected directly into amber glass vials, which were previously combusted for 4 hours at 450°C. In a separate study (Kost et al., 2022), splits of water samples on the same day and location were analyzed for stable isotopes, trace elements, carbon isotopic ratio of dissolved inorganic carbon (DIC) and cave conditions (Temperature, RH, pCO2) were recorded. The samples were shipped to ETH Zurich and stored in the dark at 4°C before measurement. Measurements of bedrock thickness for all sampling locations (Table 1) were carried out with a modified Leica Disto X310 (Heeb, 2009, 2010). The sampling frequency was chosen to identify seasonal scale changes in drip water fluorescence. Given the length of the entire time series (only one year), longterm trends and interannual variability cannot be evaluated. The bi-weekly or monthly sampling is also not designed to capture the effect of fast-changing fissure flows; however, with one exception (*FOR*), the sampled sites are classified at the boundary between seepage flow and seasonal drip based on the variation in drip rate, suggesting a dominant matrix flow component (Kost et al 2022).

Drip Water Absorbance and Fluorescence Measurements

Drip water samples were stored at 4°C in a refrigerator unit without other biological samples or organic solvents. Samples were measured between one month and one year after collection and it has been double-checked that storage time does not impact the results by re-measuring selected older samples (Supplementary Figure 1). Previous studies showed a removal of especially tryptophan-like fluorescence after filtering the samples (Baker et al., 2007). Therefore, because no large colloids were expected in our drip waters and we were interested in total fluorescence reaching the speleothem, we did not filter the samples.

Drip water absorbance spectra and fluorescence excitation-emission matrices (EEM) were measured simultaneously with a Horiba AquaLog spectrofluorometer using 4 s integration time and a step-size of 5 or 3 nm, depending on measurement day. Quartz cuvettes with a pathlength of 1x1 cm were used and rinsed several times with nanoQ water between each measurement. During post-processing EEMs with 3 nm resolution were converted to the coarser 5 nm resolution by bicubic interpolation to enable PARAFAC analysis and increase comparability between individual measurements days. EEMs were exported from the R1/C1 AquaLog output with respective excitation and emission wavelengths of 240-600 nm and 240-800 nm. Further post-processing included NanoQ water blank subtraction, inner-filter effect correction, Raman/Rayleigh scatter removal and Raman normalization performed with eemR (Massicotte, 2019). EEMs were visualized using the scientific colour map *batlow* (Crameri et al., 2020). Intensity is given in normalized raman units (R. U.) and variability of data is expressed in the form of 1 standard deviation.

Confocal Laser Scanning Microscopy

Solid-phase fluorescence in three active stalagmites and one bedrock sample was investigated with confocal laser scanning microscopy (CLSM). Measurements were performed at Scientific Center for Optical and Electron Microscopy (ScopeM) at ETH Zurich using an Olympus Fluoview 3000 and the methodology of Sliwinski and Stoll (2021). The instrumental settings result in an optical slice thickness of less than 10 μm with an 10x objective. An excitation wavelength of 488 nm and detection window of 490-590 nm were used, and resulted in an optical slice thickness of less than 10 µm with an 10x objective. The instruments minimum excitation wavelength is 405 nm, so UV excitation in solid state was not possible. Retrieved images were mirrored to represent the original orientation and a scale bar was added using Fiji (Schindelin et al., 2012).

Liquid-Phase Fluorescence Measurement of Bedrock Sample

Contribution of the bedrock to drip water fluorescence was investigated by dissolving three times 2 mg aliquots of drilled powder samples in 4.5 ml of 0.025 M HCl, analogous to Pearson et al. (2020). The aqueous solution was brought to a pH of 5-7 by titration with NaOH. Dissolved bedrock absorbance spectra and fluorescence EEM were post-processed identical to drip water and measured on the same instrument, but with an integration time of 10 s and a step size of 5 nm.

Numerical Analysis Methods

PARAFAC modeling

PARAllel FACtor (PARAFAC) analysis (Stedmon and Bro, 2008) was used to investigate DOM fluorescence variability in the spatial and temporal domain. Over the last decade, PARAFAC modeling has become a standard approach for EEM interpretation due to the possibility of recognizing site-specific peaks instead of referring to general literature (Coble et al., 2014). A global five-component model was computed from 65 corrected EEMs by staRdom (Pucher et al., 2019) with non-negative constraints, a model tolerance of $1e^{-8}$, 40 models and 10'000 maximum iterations. All models converged with these settings and no additional outliers were found by visual. Validation with a regular split-half analysis was not considered statistically robust due to the high variability between the sites and small sample size < 100 (Pucher et al., 2019). Instead, separate local PARAFAC models of the five main sampling sites were computed with fewer components due to the small sample sizes of 9-13 samples. To compare local models to the global five-component model, shape-sensitive congruencies (SSC) (Wünsch et al., 2019) were computed for each combination to quantify similarities between the individual components in the two models (Supplementary Figure 2).

The final PARAFAC model was uploaded to OpenFluor database (Murphy et al., 2014b) to compare peaks with published PARAFAC models. Model stability was assessed with the core consistency diagnostics (CORCONDIA) by Bro and Kiers (2003) and was found to be 79.65%. PARAFAC components were visualized using the scientific colour map *ajolla* (Crameri et al., 2020).

Calculation of Absorption Spectra and Slope Ratio

In addition to the fluorescent measurement, optical properties of DOM can be characterized by joint absorption measurements with the Aqualog spectrofluometer. The fraction of total DOM that absorbs UV and visible light, chromophoric dissolved organic matter, can overlap with the fraction of fluorescent DOM, but is not necessarily the same and analysing absorbance separately adds additional information about the origin and composition of the samples. To this purpose, absorbance measured with Aqualog was converted to the absorption coefficient α following Beer's law (Supplement Eq. 1).

We have used the absorption α as a quality test, whether the unfiltered samples are optically dilute enough. Values for α were well below 0.1 for all samples and measured wavelengths except for *GRA* on 7.8.2020, which showed evidence of mud contamination already during collection and was subsequently treated as outlier. Two samples containing negative absorbance values have also been disregarded for absorbance analysis.

From the entire absorption spectra, a slope ratio between a shorter (275-295 nm) over a longer (350-400 nm) wavelength region was computed analogous to Helms et al. (2008). The two slopes, $S_{275-295}$ and $S_{350-400}$, were computed by fitting a linear model through the natural logarithm of the absorption spectra values in the respective wavelength regions. By convention, positive slope values are given for a decrease with higher wavelengths in order to fit the expected exponential decay.

RESULTS AND DISCUSSION

Dominant Modes of Drip Water Fluorescence and their Attribution

The principal peaks and modes of variability in fluorescence across all collected drip water samples are identified with PARAFAC analysis. We present a five-component model, which explains 88% of the total variance within the entire data set (Fig. 2a and Table 2) and serves as a base template for further interpretation of the individual locations. The components C1-C5 are normalized to unit intensity and are ordered by the fraction of variance explained.

The dominant feature of odd PARAFAC components (C1,C3,C5) is the occurrence of a double peak within the EEM (Fig. 2a). C1 shows two excitation peaks (Ex_{max}) at 240/320 nm and an emission maximum (Em_{max}) at 405 nm, which are traditionally assigned to Peaks A_c and C (Coble et al., 2014). These peaks have been widely recognized as humic-like components with high molecular weight and aromatic organic compounds derived from plant litter (Stedmon and Cory, 2014; Coble et al., 2014). In this study, these are thought to originate mostly from vegetation above the cave and containing compounds from plant litter such as lignin. The components C3 (Em_{max} = 305 nm, Ex_{max} = 240/280 nm), and C5 (Em_{max}=455 nm, Ex_{max} =265/370 nm), appear to be blue and red shifted versions of C1, respectively. C5 exhibits a shift towards longer wavelengths and similar patterns have been attributed to soil fulvic acid (Yamashita and Jaffé, 2008) and terrestrial higher plants (Cory and McKnight, 2005). Shifting of wavelengths towards a more blue spectrum (i.e., shorter wavelengths) is likely to appear due to breaking of aromatic bonds in the original compounds by microbial activity (degradation). C3, shifted towards shorter wavelengths, possibly indicates the presence of older and/or more processed material. This kind of fluorescence is often present in marine planktonic environments, but has also been shown to be produced within the lower soil or epikarst by planktonic, heterotrophic bacteria feeding from plant litter (Xia et al., 2022) and is consistent with EEM of fossil (degraded oil) compounds (Zhou et al., 2013). We have dissolved the organic-rich bedrock to investigate a possible contribution of indigenous fluorescence due to bedrock leaching. A comparison of the bedrock-derived EEM (Fig. 2b) with PARAFAC peak wavelengths shows a strong similarity to C3. Therefore, we propose that fluorescent material within the organic-rich bedrock, which potentially is released during bedrock leaching, could be a major source for C3 drip water fluorescence. To our knowledge, such a contribution of fossil organic matter to drip water fluorescence has not been discussed in literature previously.

The two even components (C2, C4) both contain single peaks with low Ex-Em wavelengths and narrow Ex/Em spectra, which has been attributed to organic compounds with a lower degree of conjugation such as microbially produced amino acids (Coble et al., 2014), microbial metabolism (Elliott et al., 2006), but also plant-derived simple phenols, indoles and tannins (Aiken 2014).

On comparison with the OpenFluor database (Murphy et al., 2014b), spectra similar (similarity scores in Ex and Em > 0.95) to C2 have occurred in cold (arctic) water surroundings, described as tyrosine-like (Chen et al., 2018), but have also been found in EEMs from melted ice cores and described as more processed microbial signal and tannin-like (Dandrilli and McConnell, 2021). While a tannin input signal from eucalyptus trees above the cave can't be excluded, we find microbial activity here the favorable explanation, because the observed seasonal variability of C2 is more similar to the microbially-altered C3 and C4 components than to C1 and C5, attributed to higher plants. Moreover, C4 spectrum is similar to the amino acid phenylalanine, which has been measured isolated by Wünsch et al. (2015). Phenylalanine is a rather hydrophobic compound, e.g produced by algae/bacteria and consequently expected to be a rather local signal originating from the lower soil/epikarst.

Characterisation of dissolved organic matter in cave drip water by EEM is limited, because EEM spectral peaks do not have unique sources and cannot unambiguously be attributed to single compounds. Additionally, PARAFAC modeling may create artifacts instead of biologically relevant signals, and changing experiment conditions (e.g. pH or temperature of drip waters) can influence the peak intensities and positions (Aiken, 2014). Nevertheless, as demonstrated by numerous applications of EEM and PARAFAC in surface waters, the combination of EEM measurements and PARAFAC modeling can be used successfully to describe properties of drip water fluorescence in more detail, with a comparably rapid measurement method. The PARAFAC model reveals several, distinct fluorescent peaks of both, humic-like and microbial origin. Specifically mentioned should as well be the absence of a further humic-like peak, often present in soils (UVC humic-like, Cuss et al. (2019)). Our C5 peak might contain some of this signal, but it is much weaker than would be expected. Based on studies investigating active carbon adsorption (Philibert et al., 2022), we suggest that this component might be preferentially adsorbed on the bedrock and this is the reason why it is missing in the here presented PARAFAC model. Future sampling including soil water would help clarify the relative contributions of soil and karst fluorescent organic matter. In combination with the here presented fossil contribution, this points towards a rather complex interaction between karst and drip water fluorescence, which will also be reflected in the speleothem. More specific information on the compounds present and their origin could be provided by future studies employing ESI-FTIR-MS (Lechleitner et al., 2017) or LC-OCD and characterizing the microbiology of the drip waters.

Spatial Variation of Drip Water Optical Properties and Relationship to Cave Setting

Drip water optical properties, summarized in Table 1, vary substantially between sampling locations. Overall mean fluorescence over the entire EEM region ranges from 10.88 +/- 0.23 R.U. (*MUS)* to 47.40 +/- 13.34 R.U. (*FOR*). The absorption coefficient of UV and visible light shows an exponential decrease with increasing wavelength across sampling locations (Fig. 3a). The observed decrease of the absorption coefficient is fast compared to samples from the surface or swamps (e.g. Helms et al. (2008)), likely due to the higher amount of filtering occurring in the carbonate aquifer. In *PLA* and *GLO* the median absorption spectra further show secondary peaks around 295 nm and 350 nm, respectively. These peaks could theoretically occur due to spectral interferences with larger colloids, but overall absorption coefficients of our samples are below < 0.1 m^{-1}. Absorption coefficients in this bandwidth could also be altered by compounds such as tryptophan or uric acid, which show local deviations in this wavelength region, when measured in isolation (Spangenberg et al., 2021). *PLA* is located below pasture and a doline; the presence of uric acid, originating from cattle, seems therefore plausible, but would need to be confirmed by future testing of uric acid by liquid chromatography-mass spectromety. *PLA* also has a significantly different slope ratio ($p<0.05$, Tukey-test), because the spectral slope $S_{275-295}$ is negative for *PLA* due to the secondary peak (Fig 3b). Although a negative $S_{275-295}$ value is a deviation from the expected exponential decay, similar features have been found in cave spring waters previously (Birdwell and Engel, 2010).

Plotted by sampling location, the average and standard deviation fluorescence EEM plots show substantial variations in peak distribution (Fig. 4). A key influence in our data set are the properties of overlying land cover (Fig. 1), featuring a gradient from dominantly forest (*FOR, SNO*), to bushes (*GLO, GRA*) and pasture (*PLA,MUS,SKY*) vegetation. Sampling locations *FOR* and *SNO* exhibit both similar average patterns and variability, with the dominant contribution from the humic-like components C1 and C5 (Fig. 4a,b). Above these locations, oak and eucalyptus trees dominate, therefore, the strong humic-like fingerprint is consistent with a higher amount of plant litter and soil products expected to be transported to the respective drip sites. In contrast, “protein-like” C2, C4 and also C3 (“fossil-like”) are rather low.

GLO and *GRA,* located in shallow depths and covered by ferns and singular trees, exhibit comparable total fluorescence, but much greater contribution of C2 and C4. *PLA* and *MUS* feature the lowest total fluorescence and very limited variability. *PLA* is covered by grass/pasture and *MUS* by ferns and singular trees. Despite similar landcover at *PLA* and *SKY, SKY* features higher overall fluorescence.

Fluorescence is generally expected to decrease with longer transport and residence time, since the organic matter can be degraded by microbial activity (Fairchild and Baker, 2012) and especially humic-like compounds are likely to adsorb on the bedrock (Jin and Zimmerman, 2010). Within our data set, depth is not a dominant control on humic-like fluorescence (Fig. 5a). Highest values are found in FOR and SNO, covered by forest, with a cover thickness of 14.35 m - 14.47 m. In contrast, humic-like fluorescence is lower in the shallow locations *GLO, GRA* and no decrease can be found compared to the deepest locations *PLA* and *SKY*. Yet, for sites of comparable landcover (*GLO, GRA, MUS*), the deepest site (*MUS*) does feature lower total fluorescence which could be due to greater degradation in transit to the deeper site. However, these three sites feature similar total C1+C5 fluorescence; therefore, it is also possible that instead of a depth driven process, the additional livestock activity at *GLO* and *GRA* may contribute to the additional C2, C3, and C4 intensity relative to *MUS.*

In this setting, the variance of drip water $\delta^{18}O$ may be useful indicator of drip water residence time (Kost et al. 2022). This is because individual rain events feature considerable $\delta^{18}O$ variability (Stoll et al., 2015; Moreno et al., 2020), but mixing within the karst reservoir leads to dampening of this signal to varying degrees at different drip sites. The greatest dampening of event scale variation, ie. those with lowest variance in drip water $\delta^{18}O$, are inferred to be characterized by the longest residence times and greatest mixing of infiltration events. Here, the $\delta^{18}O$ variance is calculated only for drip water sites monitored for at least 9 samplings over at 9 month period, and is notably much greater for the *FOR* location than for the other calculated sites (*PLA, SKY, GLO, GRA*). The site with much higher $\delta^{18}O$ variance and shorter residence time, *FOR*, features higher total C1+C5 fluorescence, compared to other sites with longer residence time Fig. 5b. We have also calculated the ratio C3/(C5+C1) to assess the relative significance of reworked or fossil DOM relative to fresher humic- and fulvic-like inputs. This ratio correlates strongly with the humification index, which has also previously been used to estimate the ages of organic matter (Ohno, 2002). The C3/(C5+C1) ratio is lowest for the *FOR* site of shortest reservoir time, consistent with least microbial consumption and/or more adsorption of high-molecular weight components (Fig. 5c). These trends are consistent with observations elsewhere that longer residence times lead to increased DOM processing through microbial transformation and adsorption reactions (Blyth et al., 2016; Lechleitner et al., 2017).

Additionally, the water flux may influence the fraction of input fluorescence which arrives at the cave drip site. Although at similar depth and reservoir mixing inferred from $\delta^{18}O$ variance, the much lower driprate of *PLA* (1.22+/- 0.916 ml/min) than *SKY* (89.22 +/- 24.25 ml/min) correlates with a much lower average total fluorescence intensity (Fig. 4b). The very high flux at *SKY* may saturate the absorbance capacity of karst host rock. Conversely, a lower drip rate and flux at *PLA* may result in a higher fraction of dissolved fluorescence components adsorbed by karst host rock and hence lower concentrations emerging in cave drip water.

The fluorescent results therefore suggest the potential for multiple land surface origins of the fluorescence components from humic and fulvic vegetation signals as well as potential livestock contributions, further modified during transport through the karst system by microbial reworking and adsorption on karst host rock (Fig. 6). Our spatial trends in total fluorescence and its composition therefore suggest that at comparable bedrock depth, higher density of trees and shorter water residence times favor higher relative contribution of fluorescence from humic-like and fulvic-like sources. Fluorescence components more likely of microbial origin dominate at sites with longer water residence times. For sites of comparable landcover and residence time, higher drip water flux (drip rate) correlates with a higher total fluorescence.

Temporal Variation of Fluorescence and Relation to Climate

Temporal variation in fluorescence components at different locations

At a given drip site, the PARAFAC model components C1 and C5 feature more constant concentrations over the year without strong seasonality (Fig. 7). In contrast, C2 and C4 intensity consists of short-lived peaks and varies substantially on the seasonal timescale in most monitored locations, especially in *GLO* and *GRA*. C3 appears more constant in some locations, but variable in other sites. Dips in protein-like fluorescence (C2,C4), e.g. in October 2020, occur often concurrently across sampling sites. In contrast, C3 peaks do not occur at the same time across drip sites, e.g. increased values in location *FOR* in autumn are contrasted by especially low C3 values in *SKY*. *FOR*, which is the more shallow sampling site and covered with denser vegetation, likely featuring rapid water transmission and shorter reservoir times inferred from its high $\delta^{18}O$ variance, might be prone to receive an increased in-flux of older soil material, e.g. from fissure flow. Despite the significant short term variation of some trace elements, consistent with mixture of matrix and fissure derived water (Kost et al., 2022), components C1,C3 and C5 variability is smoothed and generally, humic-like fluorescence is present over the entire year. This constancy might be related to longer water residence times and well-mixed reservoirs, but it may also or additionally reflect a buffering of the concentration of humic components by sorption processes in the karst reservoir. Abiotically, humic-like compounds are preferentially adsorbed by the carbonate bedrock, while during low input of humic-like compounds, a large portion of the compounds are likely to desorb again from the bedrock (Jin and Zimmerman, 2010). In the presented data set, this process together with the release of indigenous organic matter from bedrock, might have weakened a potential seasonal cycle, leading to basically constant values of humic-like fluorescence.

Relationship of fluorescence to rainfall and temperature

Relevant for the interpretation of the fluorescent signal within speleothems is further the dependence on climatological parameters such as temperature and precipitation. We investigate this hypothesis by comparing the fluorescence dataset to climatological data from the nearby weather station Llanes (4.2km NE of the cave, at the coast). Two equally-sized groups of dry and wet conditions are compared for each location based on total rainfall amount in the 10 days prior to sampling (Fig. 8, top row). The humic-like and fulvic-like components C1 and C5 are higher during wet conditions only for the location *FOR,* whereas all other locations show no change between the wet vs dry conditions, and *PLA* shows lower C5 for wet conditions. For C3, *FOR* shows higher values in wet conditions, whereas other sites (*PLA, SKY*) show increased values for dry conditions or no difference (*GRA, GLO*). This contrasting behavior at *FOR* may reflect an aged soil source of C3 at this site and its fast transmission due to the low reservoir time of FOR drip water, versus deeper sites where C3 may be more significantly sourced from fossil bedrock OM and therefore decoupled from the precipitation regime.

In contrast, microbial components C2, C4 are enhanced for dry conditions across all drip sites. Here, the difference in C4 between the two conditions is more pronounced for shallow locations *FOR* and *GLO*, than for *PLA* and *SKY*. Because all monitored sites continued dripping throughout the 16 month monitoring period, we infer that water is present continually within the karst. However, we hypothesize that the presence of cavities in semi-dry aquifers enhance the conditions for microbial life (C2,C3,C4). Shallow locations might react more readily because they dry out faster and carbon sources for microbes might be more abundant. An alternative interpretation would be that the microbial population and its contributions are diluted during wet periods. Similar results, an increased presence of autochthonous microbial fluorescence for drier conditions, have been found experimentally for karstic subsurface-environments (Xia et al., 2022). The here presented groups are too small for statistical tests, but a t-Test on the difference between the means of humic components C1,C5 and microbial components C2,C4 over data from all locations yields significantly higher values in dry conditions for microbial components (p-value= 0.021, Supplementary Figure 3).

In contrast to precipitation, with the same methodology no effect of ambient temperature on the fluorescence fingerprint could have been detected (Fig. 8, bottom row), which is justified by the constant temperature conditions present within the karst (T_{mean}=13.96 °C, average seasonal variation with SD $\pm 0.32°C$) (Fig. 8, bottom row).

Relationship of fluorescence to soil respiration, bedrock dissolution, and chelated metal transport

We compare the fluorescence signals with indicators of karst processes measured on the same drip water samples. The carbon isotopic ratio of dissolved inorganic carbon (DIC) in drip water is interpreted as an indicator of the soil and epikarst CO2 which in turn is driven by the aggregate autotrophic and heterotrophic respiration rate (Kost et al., 2022). More negative $\delta^{13}C_{DIC}$ indicates higher respiration rates. At the shallow and rapid transmitting *FOR* location, the higher soil and epikarst respiration rates coincide with the highest concentrations of C1 (and C5), suggesting either that that high respiration rates contribute to high production of humic-like breakdown products, or that conditions optimal for maximizing respiration are also optimal for maximizing the release of humic-like components to waters (Fig. 9a). We suspect that at the other sites with long data series (*SKY, PLA, GLO, GRA*), longer water reservoir times may attenuate the seasonal signal in dissolved fluorescence leaving the soil layer relative to the cycle of $\delta^{13}C_{DIC}$. This is because $\delta^{13}C_{DIC}$ is not sensitive to water residence time, when it is set by continued CO_2 exchange with water throughout the infiltration pathway by deep-rooted trees (Breecker et al., 2012). No significant relationship is observed between the $\delta^{13}C_{DIC}$ and the fraction of fresher versus the more degraded compounds (C3:(C1+C5) ratio) nor the concentration of the C2 and C4 compounds, at any site.

Within a given dripsite, the concentration of Sr has been proposed as an indicator of the intensity of bedrock dissolution, because all drip water Sr is bedrock sourced, and the concentration of Sr is not appreciably affected by precipitation of $CaCO_3$ prior to sampling of drip water (Kost et al., 2022). Across all of the sampled sites, there is a general weak positive correlation between the Sr concentration and the concentration of C1, driven primarily by the higher concentrations in the FOR site compared to other sites (Fig. 9b). This correlation may arise because greater soil and epikarst respiration and CO_2 are required to attain greater degrees of bedrock dissolution, and these higher rates of respiration result in greater production of humic-like components. The forested vegetation of the *FOR* site would especially favor high respiration rates. A similar correlation is observed for Ca (Supplementary Figure 4). No significant correlation is observed between the bedrock dissolution and the concentration of C3, or the ratios of other components.

Highly insoluble transition metals and REE-like elements such as Cu or Y are inferred to be transported in drip waters as complexes with organic ligands such as humic and fulvic acids (Hartland et al., 2014; Hartland and Zitoun, 2018), and in stalagmites, seasonal layers of enhanced fluorescence often coincide with elevated concentrations of these elements (Sliwinski and Stoll, 2021). However, a comparison of C1 and C5 concentrations with the concentration of drip water Cu (Fig. 9c) (or Y; Supplementary Figure 4) reveals no significant correlations within a given site or across all sites. This lack of relationship suggests that the Cu and Y concentration in drip water may be controlled by more unique components of the dissolved organic carbon pool than resolved by the C1 or C5 fluorescence, that fluorescent DOM present is not necessarily attached to colloids, or that other controls of selective scavenging of either Y or organic ligands decouple any initial relationship. The precise relationship between Y (and transition metal transport) and dissolved organic components in drip waters may require further analysis in typical karst settings, as the relationships to date have been explored most rigorously in a hyperalkaline cave setting (Hartland et al., 2014).

Relating Drip water fluorescence and speleothem fluorescence

Annual scale fluorescent lamination has been reported in mid-latitude stalagmites (McGarry and Baker, 2000; Kwiecien et al., 2022; Luetscher et al., 2021; Sliwinski and Stoll, 2021) from this and other caves, and our (CLSM) images (Fig. 10 a-c) reveal some sectors in the actively growing stalagmite from beneath the *SKY*, and *SNO* drip locations with fine scale lamination which may be annual to subannual according to available age models from ^{14}C (Sliwinski et al., 2022). These rapidly growing stalagmites feature high porosity and many crystal defects, which contribute to lateral discontinuity in fluorescent lamination, as described in previous studies (Sliwinski and Stoll, 2021; Sliwinski et al., 2022). In our study with CLSM, the selected excitation wavelength is 488 nm. Based on our analysis of dissolved fluorescence, this range is suitable to stimulate fluorescence in the humic-like and fulvic-like region of C1 or C5, but not as significantly for C2, C3, or C4. Nonetheless, comparing solid state and dissolved fluorescence is not straightforward. The polished bedrock sample, dominated by C3-like component in dissolved form, also indicates pronounced fluorescence, concentrated in certain sectors, by this same 488 nm excitation wavelength in the solid state CLSM analysis of the stalagmites (Fig. 10d), suggesting that this bedrock component, if present without further modification, would also be detected in our stalagmite CLSM analyses.

While the prevailing hypothesis for fluorescent laminae in speleothems invokes an autumnal pulse in fluorescent components (along with colloidally transported metals) with the onset of autumnal rains and infiltration after a dry summer, our sampling has not detected any seasonal pulses of humic-like or fulvic-like fluorescence in autumn or any other season in the drip water at any monitored sites (Fig. 7), and we also do not detect a relationship between C1 or C5 with precipitation at *SKY* (Fig. 8). In previous studies, fluorescent lamination has been attributed to humic- and fulvic-like components (e.g., McGarry and Baker, 2000; Pearson et al., 2020), although we are aware of no full EEM characterization of the speleothem fluorescence from annually laminated stalagmite samples. Because of the low concentrations of organic matter, we have not been able to obtain EEM spectra of our actively growing stalagmites, so the conventional inference of humic- and fulvic-like source components of the fluorescent laminae cannot be tested in these active stalagmites. Given the absence of any seasonal variation in humic-like and fulvic-like drip water concentrations at our cave setting, several alternative processes may contribute to the formation of annual to subannual fluorescent laminae. First, if the fluorescent lamina were dominated by the C1 and C5 components, which have constant concentrations in drip water, it is possible that a concentrated fluorescent layer reflects not changes in the delivery of fluorescent components, but rather variable dilation of the fluorescence in the stalagmite as a function of the $CaCO_3$ deposition rate. An analogous mechanism has been described for the generation of a seasonal Y peak in stalagmites, whereby periods of slower stalagmite growth distribute an otherwise constant Y (or fluorescence) flux over a shorter distance in the stalagmite, generating higher average concentrations in the slower growth portion of the year (Sliwinski et al., 2022). Based on calculations from the monitored drip water Ca concentrations and the cycle in cave air pCO_2, stalagmite growth at SKY is simulated to occur rapidly during the winter season, and slowly during the summer season, with brief periods of negligible growth simulated during the spring and fall (Kost et al., 2022). In such a stalagmite growth regime, the slow growth during summer could lead to enhanced fluorescent intensity in the summer and weaker fluorescent intensity in the winter layer. In the case that fluorescent laminae were dominated by C1 and C5 like components, an alternative mechanism for the development of a fluorescent laminae could be an increased absorption or trapping efficiency of the fluorescent components in the stalagmite during one season, due to change in factor such as drip water pH or residence time on the stalagmite. Here, further experiments testing the affinity of different organic ligands to Ca and trace elements would be beneficial for interpretation.

In some of our monitored drip waters (*GLO, SKY*, to lesser extent *FOR*), the C3 component exhibited greater temporal variation than C1 or C5. If this component were the main source of fluorescence in the laminae, the variations in C3 concentration in drip water might contribute to modest seasonal variation in speleothem fluorescence. However, the distinct drip water sites exhibited different seasons of maximum C3 fluorescence, so if this were the dominant process behind laminations, it would imply that the bright fluorescent laminae may not represent the same season in all stalagmites from a given cave. C2 and C4 components exhibit consistent increase during dry intervals, so if these components dominated the variability in the stalagmite laminae, it could contribute to systematic oscillations on annual to subannual scale. However, a further caution is that the sites in our program which exhibit large variations in C2, C3, and C4 components are also in sectors of the cave beneath at least intermittent livestock activity. We cannot assess if such variations would characterize a natural system, or if they are enhanced by the variation in livestock presence. A final possible explanation could be that the fluorescent layers are driven by a season of elevated in-situ microbial production on the stalagmite surface. Lipid distributions document a unique microbial community on the surface of stalagmites distinct from that of soil microbial communities transmitted in drip waters (Blyth et al., 2014, 2016) but it is not yet known how the microbial density of the stalagmite surface community might vary temporally and affect fluorescence.

We favor the first explanation as an important factor for the generation of annual to subannual fluorescent laminae, based on its relevance for also explaining cyclicity in colloidally transported trace elements. This process could also provide an explanation for the lack of annual to subannual scale fluorescent lamination in some active stalagmites from the cave (such as PG-2, close to the drip site *PLA*). At some drip locations, including *PLA*, stalagmite growth is modeled to occur rapidly but only during one brief part of the year (Kost et al, 2022). In such a case, there may not be variation in the deposition rate of the formed calcite, and therefore fluorescence incorporation could be homogeneous. Further characterization of the sources of fluorescent components in stalagmites featuring annual lamination will be important to test the alternative hypotheses for layer formation.

CONCLUSIONS AND IMPLICATIONS

Characterization of cave drip waters by full EEM matrices is a non-destructive, readily applied technique for which PARAFAC analysis facilitates increasingly refined interpretations and contributes to improved understanding of the natural dissolved organic matter dynamics in cave systems. We have conducted a one-year monitoring of fluorescence in drip water at a monthly resolution in a cave system with varying vegetation and land use at the surface above the cave. Our results indicate diverse fluorescence contributions characterized by a five component PARAFAC model, which likely originate from the overlying vegetation, sectors of livestock grazing above the cave, microbial processes and the fossil bedrock. The contribution of fossil organic material in bedrock to drip water fluorescence is suggested by EEMs of dissolved bedrock samples exhibiting a peak of Ex/Em 250/330 and 280/335, very similar to one of the drip water components identified by PARAFAC models. To our knowledge, this is the first study indicating a contribution of fossil fluorescent compounds to fluorescence in drip waters and potentially the precipitating speleothems.

Across this cave system, the nature of fluorescence varies significantly among drip sites characterized by different land cover and water reservoir times. Drip sites with dense tree cover and low reservoir mixing times are characterized by the highest concentrations of humic-like and fulvic-like fluorescence. Similar total fluorescence, but much lower humic-and fulvic-like components, characterized sites with longer reservoir mixing times and mixed tree and fern cover. The site with pasture above the drip site exhibited almost no humic-like fluorescence and the lowest total fluorescence. For sites of comparable landcover and residence time, higher drip water flux (drip rate) correlates with a higher total fluorescence concentration in drip water. Especially under long flow routes and long reservoir times, drip sites fed by a low water flow, may lose a greater fraction of dissolved organic matter to adsorption on karst host rock, reducing the final concentration arriving at the drip point in the cave. The role of microbiological processes in the epikarst and within the caves, merits further exploration because of the potential effect on interpretation of fluorescence properties of stalagmites.

In our data set, concentration of humic-like and fulvic-like fluorescence is constant and not significantly enhanced seasonally in any drip sites. Higher concentrations of these components accompany rainier periods only at a single drip site characterized by the shortest residence times. In contrast, tyrosine-like and protein-like components of C2 and C4, hypthesized to originate from microbial activity in the soil or epikarst, exhibit greater temporal variations in some drip sites, and increase in concentration during drier periods across all drip sites. It is unclear if this trend reflects greater microbial production during dry periods, or reduced dilution of a stable microbial population within the karst or cave during dry periods.

These findings have several important implications for the interpretation of fluorescence and fine scale annual to subannual fluorescent lamination in stalagmites. First, the surface vegetation signal of humic like and fulvic like fluorescence may dominate the drip water fluorescence signal reaching stalagmites, only in settings which feature low water reservoir times and limited microbial reworking. Our data are consistent with a greater reduction in the concentration of fluorescent compounds in very slow flow drip sites compared to fast flow, likely due to the adsorption of fluorescent compounds to host karst rock. Interpretation of the fluorescent components in stalagmites therefore needs to consider the reprocessing reactions that operate between the surface environment and the cave. Additionally, a bedrock source of fossil fluorescent material, independent of the surface landscape or climate conditions at the time of stalagmite growth, may be significant in some cave systems.

Our finding of annual to sub-annual cyclic fluorescent layers in an actively growing stalagmite beneath a drip characterized by invariant humic and fulvic-like components, challenges one conventional interpretation for the origin of fluorescent laminae by a high autumnal influx of organic matter. Our favored interpretation is that fluorescent laminae could be generated during seasons of slower stalagmite growth in which an otherwise constant concentration of fluorescent components is concentrated over a shorter distance in the stalagmite, generating higher average stalagmite fluorescence in the slower growth portion of the year. In this case, the season of maximum fluorescence may not be identical among multiple caves or even among multiple stalagmites in the same cave system, because season of stalagmite growth depend on the timing and intensity of cave ventilation which can vary both among different caves and within a given cave system. Thus, the fluorescent laminae should not be assumed to be a consistent marker of a particular season nor used to reference the attribution of a particular season to observed cycles in $\delta^{13}C$ or trace elements.

Alternatively, fluorescent laminae could be dominated by variations in the non-humic and non-fulvic components of fluorescence. Certain of these components were systematically elevated during dry intervals. If these components are most responsible for fluorescent lamination, then fluorescent laminae may represent dry periods, exactly the opposite interpretation as the conventional hypothesis. In our sites, variations in these components were not synchronous among multiple drip locations, indicating that this process could also lead to seasonally diachronous fluorescent layers in different drip settings. Nonetheless, additional monitoring studies in cave settings with less livestock influence would be important to distinguish if large variations in drip water tyrosine-like, and protein-like components also characterize systems in a more natural state. More generally, to more confidently reconcile the interpretation of fluorescent laminae in stalagmites, it will be important to identify which fluorescent components are responsible for the annual to subannual scale lamination in stalagmites by EEM or other analytical approaches. Some fluorescent components may be selectively incorporated in stalagmite calcite and therefore play a larger role than predicted by their relative contribution to the drip water fluorescence. Furthermore, it will be important to assess if the constancy of humic-like and fulvic-like drip water concentrations seen in this cave is representative of other cave systems in which annual to subannual fluorescent laminae are documented.

COMPETING INTERESTS

The authors declare that they have no known competing interests or personal relationships that could have appeared to influence the work reported in this paper.

ACKNOWLEDGEMENTS

This study was supported by ETH core funding and ETH Zürich [grant number ETH-1318-1].

DATA AND CODE AVAILABILITY

Upon acceptance of this article, all data used in the study and codes for figure compilation will be uploaded to https://github.com/lrndrs/Organics_Analysis, last access: 30 December 2022) and given in the supplement provided with the article. The compiled data set of drip water organics and chemistry will also be uploaded to PANGEA (https://www.pangaea.de/, last access: 30 December 2022) and the PARAFAC model will be published in the OpenFluor database (https://openfluor.lablicate.com, last access: 30 December 2022).

REFERENCES

Aiken, G. R.: Fluorescence and dissolved organic matter: A chemist's perspective: Chapter 2, 35–74 pp., https://doi.org/10.1017/CBO9781139045452.005, 2014.

Alberts, J. J. and Takács, M.: Comparison of the natural fluorescence distribution among size fractions of terrestrial fulvic and humic acids and aquatic natural organic matter, Org Geochem, 35, 1141–1149, 2004.

Álvarez, R., Ordóñez, A., Canteli, P., and de Miguel, E.: Unconventional gas resources in the Cantabrian Zone (NW Spain): A comprehensive preliminary assessment, Geological Journal, 54, 2608–2620, https://doi.org/10.1002/gj.3314, 2019.

Baker, A. and Genty, D.: Fluorescence wavelength and intensity variations of cave waters, J Hydrol (Amst), 217, 19–34, https://doi.org/10.1016/S0022-1694(99)00010-4, 1999.

Baker, A., Smart, P. L., Edwards, R. L., and Richards, D. A.: Annual growth banding in a cave stalagmite, Nature, 364, 518–520, 1993.

Baker, A., Smith, C., Jex, C., Fairchild, I., Genty, D., and Fuller, L.: International Journal of Speleology Annually Laminated Speleothems: a Review, Int J Speleol, 37, 193–206, 2008.

Birdwell, J. E. and Engel, A. S.: Characterization of dissolved organic matter in cave and spring waters using UV-Vis absorbance and fluorescence spectroscopy, Org Geochem, 41, 270–280, https://doi.org/10.1016/j.orggeochem.2009.11.002, 2010.

Blyth, A. J., Baker, A., Collins, M. J., Penkman, K. E. H., Gilmour, M. A., Moss, J. S., Genty, D., and Drysdale, R. N.: Molecular organic matter in speleothems and its potential as an environmental proxy, Quat Sci Rev, 27, 905–921, https://doi.org/10.1016/j.quascirev.2008.02.002, 2008.

Blyth, A. J., Jex, C. N., Baker, A., Khan, S. J., and Schouten, S.: Contrasting distributions of glycerol dialkyl glycerol tetraethers (GDGTs) in speleothems and associated soils, Org Geochem, 69, 1–10, 2014.

Blyth, A. J., Hartland, A., and Baker, A.: Organic proxies in speleothems–New developments, advantages and limitations, Quat Sci Rev, 149, 1–17, 2016.

Borsato, A., Frisia, S., Fairchild, I. J., Somogyi, A., and Susini, J.: Trace element distribution in annual stalagmite laminae mapped by micrometer-resolution X-ray fluorescence: Implications for incorporation of environmentally significant species, Geochim Cosmochim Acta, 71, 1494–1512, https://doi.org/10.1016/j.gca.2006.12.016, 2007.

Breecker, D. O., Payne, A. E., Quade, J., Banner, J. L., Ball, C. E., Meyer, K. W., and Cowan, B. D.: The sources and sinks of CO2 in caves under mixed woodland and grassland vegetation, Geochim Cosmochim Acta, 96, 230–246, 2012.

Bro, R. and Kiers, H. A. L.: A new efficient method for determining the number of components in PARAFAC models, J Chemom, 17, 274–286, https://doi.org/10.1002/cem.801, 2003.

Chen, M., Jung, J., Lee, Y. K., and Hur, J.: Surface accumulation of low molecular weight dissolved organic matter in surface waters and horizontal off-shelf spreading of nutrients and humic-like fluorescence in the Chukchi Sea of the Arctic Ocean, Science of the Total Environment, 639, 624–632, https://doi.org/10.1016/j.scitotenv.2018.05.205, 2018.

Coble, P. G., Spencer, R. G. M., Baker, A., and Reynolds, D. M.: Aquatic Organic Matter Fluorescence, 75–122 pp., https://doi.org/10.1017/cbo9781139045452.006, 2014.

Cory, R. M. and McKnight, D. M.: Fluorescence spectroscopy reveals ubiquitous presence of oxidized and reduced quinones in dissolved organic matter, Environ Sci Technol, 39, 8142–8149, https://doi.org/10.1021/es0506962, 2005.

Crameri, F., Shephard, G. E., and Heron, P. J.: The misuse of colour in science communication, Nat Commun, 11, https://doi.org/10.1038/s41467-020-19160-7, 2020.

Cuss, C. W., Donner, M. W., Noernberg, T., Pelletier, R., and Shotyk, W.: EEM-PARAFAC-SOM for assessing variation in the quality of dissolved organic matter: simultaneous detection of differences by source and season, Environmental Chemistry, 16, 360–374, https://doi.org/10.1071/EN19016, 2019.

Dandrilli, J. and McConnell, J. R.: Polar ice core organic matter signatures reveal past atmospheric carbon composition and spatial trends across ancient and modern timescales, Journal of Glaciology, 67, 1028–1042, https://doi.org/10.1017/jog.2021.51, 2021.

Delavaud, E., Cotton, F., Akkar, S., Scherbaum, F., Danciu, L., Beauval, C., Drouet, S., Douglas, J., Basili, R., Sandikkaya, M. A., and others: Toward a ground-motion logic tree for probabilistic seismic hazard assessment in Europe, J Seismol, 16, 451–473, 2012.

Fairchild, I. J. and Baker, A.: Speleothem Science: From Process to Past Environments, John Wiley & Sons, 2012.

Hartland, A. and Zitoun, R.: Transition metal availability to speleothems controlled by organic binding ligands, Geochem Perspect Lett, 8, 22–25, https://doi.org/10.7185/geochemlet.1824, 2018.

Hartland, A., Fairchild, I. J., Müller, W., and Dominguez-Villar, D.: Preservation of NOM-metal complexes in a modern hyperalkaline stalagmite: Implications for speleothem trace element geochemistry, Geochim Cosmochim Acta, 128, 29–43, 2014.

Heeb, B.: An all-in-one electronic cave surveying device, Cave Radio \& Electronics Group Journal, 72, 8–10, 2009.

Heeb, B.: A general calibration algorithm for 3-axis compass/clinometer devices, Cave Radio and Electronics Group Journal, 73, 2010.

Helms, J. R., Stubbins, A., Ritchie, J. D., Minor, E. C., Kieber, D. J., and Mopper, K.: Absorption spectral slopes and slope ratios as indicators of molecular weight, source, and photobleaching of chromophoric dissolved organic matter, Limnol Oceanogr, 53, 955–969, https://doi.org/10.4319/lo.2009.54.3.1023, 2008.

Huang, Y., Fairchild, I. J., Borsato, A., Frisia, S., Cassidy, N. J., McDermott, F., and Hawkesworth, C. J.: Seasonal variations in Sr, Mg and P in modern speleothems (Grotta di Ernesto, Italy), Chem Geol, 175, 429–448, https://doi.org/https://doi.org/10.1016/S0009-2541(00)00337-5, 2001.

IAEA/WMO: Global Network of Isotopes in Precipitation. The GNIP Database., Accessible at: http://www.iaea.org/water, 2022.

Jin, J. and Zimmerman, A. R.: Abiotic interactions of natural dissolved organic matter and carbonate aquifer rock, Applied Geochemistry, 25, 472–484, https://doi.org/10.1016/j.apgeochem.2009.12.012, 2010.

Köppen, W.: Die Wärmezonen der Erde, nach der Dauer der heissen, gemässigten und kalten Zeit und nach der Wirkung der Wärme auf die organische Welt betrachtet, Meteorologische Zeitschrift, 1, 5–226, 1884.

Kost, O., González-Lemos, S., Rodriguez-Rodriguez, L., Sliwinski, J., Endres, L., Haghipour, N., and Stoll, H.: Relationship of seasonal variations in drip water δ 13 CDIC, δ 18 O and trace elements with surface and physical cave conditions of La Vallina Cave, NW Spain, Hydrology and Earth System Sciences Disc., 1–42, https://doi.org/10.5194/hess-2022-386, 2022.

Kwiecien, O., Braun, T., Brunello, C. F., Faulkner, P., Hausmann, N., Helle, G., Hoggarth, J. A., Ionita, M., Jazwa, C. S., Kelmelis, S., Marwan, N., Nava-Fernandez, C., Nehme, C., Opel, T., Oster, J. L., Perşoiu, A., Petrie, C., Prufer, K., Saarni, S. M., Wolf, A., and Breitenbach, S. F. M.: What we talk about when we talk about seasonality – A transdisciplinary review, Earth Sci Rev, 225, 103843, https://doi.org/10.1016/j.earscirev.2021.103843, 2022.

Lakowicz, J. R.: Principles of fluorescence spectroscopy, Springer, 2006.

Lechleitner, F. A., Dittmar, T., Baldini, J. U. L., Prufer, K. M., and Eglinton, T. I.: Molecular signatures of dissolved organic matter in a tropical karst system, Org Geochem, 113, 141–149, https://doi.org/10.1016/j.orggeochem.2017.07.015, 2017.

Lindeman, I., Hansen, M., Scholz, D., Breitenbach, S. F. M., and Hartland, A.: Effects of organic matter complexation on partitioning of transition metals into calcite: Cave-analogue crystal growth experiments, Geochim Cosmochim Acta, 317, 118–137, https://doi.org/10.1016/j.gca.2021.10.032, 2021.

Luetscher, M., Moseley, G. E., Festi, D., Hof, F., Edwards, R. L., and Spötl, C.: A Last Interglacial speleothem record from the Sieben Hengste cave system (Switzerland): Implications for alpine paleovegetation, Quat Sci Rev, 262, https://doi.org/10.1016/j.quascirev.2021.106974, 2021.

Massicotte, P.: eemR: tools for pre-processing emission-excitation-matrix (EEM) fluorescence data, R package version, 1, 2019.

McGarry, S. F. and Baker, A.: Organic acid fluorescence: Applications to speleothem palaeoenvironmental reconstruction, Quat Sci Rev, 19, 1087–1101, https://doi.org/10.1016/S0277-3791(99)00087-6, 2000.

McKnight, D. M., Boyer, E. W., Westerhoff, P. K., Doran, P. T., Kulbe, T., and Andersen, D. T.: Spectrofluorometric characterization of dissolved organic matter for indication of precursor organic material and aromaticity, Limnol Oceanogr, 46, 38–48, https://doi.org/10.4319/lo.2001.46.1.0038, 2001.

Moreno, A., Iglesias, M., Azorin-Molina, C., Pérez-Mejías, C., Bartolomé, M., Sancho, C., Stoll, H., Cacho, I., Frigola, J., Osácar, C., Muñoz, A., Delgado-Huertas, A., Blade, I., and Vimeux, F.: Spatial variability of northern Iberian rainfall stable isotope values: Investigating climatic controls on daily and monthly timescales, Atmospheric Chemistry and Physics Discussions, 1–34, https://doi.org/10.5194/acp-2020-861, 2020.

Mudarra, M., Andreo, B., and Baker, A.: Characterisation of dissolved organic matter in karst spring waters using intrinsic fluorescence: Relationship with infiltration processes, Science of the Total Environment, 409, 3448–3462, https://doi.org/10.1016/j.scitotenv.2011.05.026, 2011.

Murphy, K. R., Bro, R., and Stedmon, C. A.: Chemometric Analysis of Organic Matter Fluorescence, 339–375 pp., https://doi.org/10.1017/cbo9781139045452.016, 2014a.

Murphy, K. R., Stedmon, C. A., Wenig, P., and Bro, R.: OpenFluor- An online spectral library of auto-fluorescence by organic compounds in the environment, Analytical Methods, 6, 658–661, https://doi.org/10.1039/c3ay41935e, 2014b.

O'Brien, B. J.: 'After -glow' of cave calcite, National Speleological Society, 18, 50–51, 1956.

Ohno, T.: Fluorescence inner-filtering correction for determining the humification index of dissolved organic matter, Environ Sci Technol, 36, 742–746, https://doi.org/10.1021/es0155276, 2002.

Orland, I. J., Bar-Matthews, M., Ayalon, A., Matthews, A., Kozdon, R., Ushikubo, T., and Valley, J. W.: Seasonal resolution of Eastern Mediterranean climate change since 34ka from a Soreq Cave speleothem, Geochim Cosmochim Acta, 89, 240–255, https://doi.org/10.1016/j.gca.2012.04.035, 2012.

Pearson, A. R., Hartland, A., Frisia, S., and Fox, B. R. S.: Formation of calcite in the presence of dissolved organic matter: Partitioning, fabrics and fluorescence, Chem Geol, 539, 119492, https://doi.org/10.1016/j.chemgeo.2020.119492, 2020.

Peel, M. C., Finlayson, B. L., and McMahon, T. A.: Updated world map of the Köppen-Geiger climate classification, Hydrol Earth Syst Sci, 11, 1633–1644, https://doi.org/10.5194/hess-11-1633-2007, 2007.

Perrette, Y., Delannoy, J. J., Desmet, M., Lignier, V., and Destombes, J. L.: Speleothem organic matter content imaging. The use of a Fluorescence Index to characterise the maximum emission wavelength, Chem Geol, 214, 193–208, https://doi.org/10.1016/j.chemgeo.2004.09.002, 2005.

Philibert, M., Luo, S., Moussanas, L., Yuan, Q., Filloux, E., Zraick, F., and Murphy, K. R.: Drinking water aromaticity and treatability is predicted by dissolved organic matter fluorescence, Water Res, 220, 118592, 2022.

Proctor, C. J., Baker, A., Barnes, W. L., and Gilmour, M. A.: A thousand year speleothem proxy record of North Atlantic climate from Scotland, Clim Dyn, 16, 815–820, https://doi.org/10.1007/s003820000077, 2000.

Pucher, M., Wünsch, U., Weigelhofer, G., Murphy, K., Hein, T., and Graeber, D.: StaRdom: Versatile software for analyzing spectroscopic data of dissolved organic matter in R, Water (Switzerland), 11, 1–19, https://doi.org/10.3390/w11112366, 2019.

Quiers, M., Perrette, Y., Chalmin, E., Fanget, B., and Poulenard, J.: Geochemical mapping of organic carbon in stalagmites using liquid-phase and solid-phase fluorescence, Chem Geol, 411, 240–247, https://doi.org/10.1016/j.chemgeo.2015.07.012, 2015.

Ramseyer, K., Miano, T. M., D'Orazio, V., Wildberger, A., Wagner, T., and Geister, J.: Nature and origin of organic matter in carbonates from speleothems, marine cements and coral skeletons, Org Geochem, 26, 361–378, https://doi.org/10.1016/S0146-6380(97)00008-9, 1997.

Reynolds, D. M.: The Principles of Fluorescence, 3–34 pp., https://doi.org/10.1017/cbo9781139045452.004, 2014.

Rutlidge, H., Baker, A., Marjo, C. E., Andersen, M. S., Graham, P. W., Cuthbert, M. O., Rau, G. C., Roshan, H., Markowska, M., Mariethoz, G., and Jex, C. N.: Dripwater organic matter and trace element geochemistry in a semi-arid karst environment: Implications for speleothem paleoclimatology, Geochim Cosmochim Acta, 135, 217–230, https://doi.org/10.1016/j.gca.2014.03.036, 2014.

Rutlidge, H., Andersen, M. S., Baker, A., Chinu, K. J., Cuthbert, M. O., Jex, C. N., Marjo, C. E., Markowska, M., and Rau, G. C.: Organic characterisation of cave drip water by LC-OCD and fluorescence analysis, Geochim Cosmochim Acta, 166, 15–28, https://doi.org/10.1016/j.gca.2015.05.042, 2015.

Schindelin, J., Arganda-Carreras, I., Frise, E., Kaynig, V., Longair, M., Pietzsch, T., Preibisch, S., Rueden, C., Saalfeld, S., Schmid, B., and others: Fiji: an open-source platform for biological-image analysis, Nat Methods, 9, 676–682, 2012.

Shopov, Y. Y., Ford, D. C., and Schwarcz, H. P.: Luminescent microbanding in speleothems: High-resolution chronology and paleoclimate, Geology, 1994.

Sliwinski, J. T. and Stoll, H. M.: Combined fluorescence imaging and LA-ICP-MS trace element mapping of stalagmites: Microfabric identification and interpretation, Chem Geol, 581, 120397, https://doi.org/10.1016/j.chemgeo.2021.120397, 2021.

Sliwinski, J. T., Kost, O., Endres, L., Iglesias, M., Haghipour, N., González-Lemos, S., and Stoll, H. M.: Exploring soluble and colloidally transported trace elements in stalagmites: the strontium-yttrium connection, Geochim Cosmochim Acta, https://doi.org/https://doi.org/10.1016/j.gca.2022.12.023, 2022.

Spangenberg, M., Bryant, J. I., Gibson, S. J., Mousley, P. J., Ramachers, Y., and Bell, G. R.: Ultraviolet absorption of contaminants in water, Sci Rep, 11, 1–8, 2021.

State Meteorological Agency of Spain: AEMET OpenData, Spain, 2021.

Stedmon, C. A. and Bro, R.: Characterizing dissolved organic matter fluorescence with parallel factor analysis: a tutorial. (2008) 6:572-579, 2008.

Stedmon, C. A. and Cory, R. M.: Biological Origins and Fate of Fluorescent Dissolved Organic Matter in Aquatic Environments, Aquatic Organic Matter Fluorescence, 278–300, https://doi.org/10.1017/cbo9781139045452.013, 2014.

Stoll, H., Mendez-Vicente, A., Gonzalez-Lemos, S., Moreno, A., Cacho, I., Cheng, H., and Edwards, R. L.: Interpretation of orbital scale variability in mid-latitude speleothem δ18O: Significance of growth rate controlled kinetic fractionation effects, Quat Sci Rev, 127, 215–228, https://doi.org/10.1016/j.quascirev.2015.08.025, 2015.

Wilkinson, K. J., N~gre, J.-C., and Buffie, J.: Contaminant Hydrology Coagulation of colloidal material in surface waters: the role of natural organic matter, Journal of Contaminant Hydrology, 229–243 pp., 1997.

Wünsch, U. J., Murphy, K. R., and Stedmon, C. A.: Fluorescence quantum yields of natural organic matter and organic compounds: Implications for the fluorescence-based interpretation of organic matter composition, Front Mar Sci, 2, 1–15, https://doi.org/10.3389/fmars.2015.00098, 2015.

Wünsch, U. J., Bro, R., Stedmon, C. A., Wenig, P., and Murphy, K. R.: Emerging patterns in the global distribution of dissolved organic matter fluorescence, Analytical Methods, 11, 888–893, https://doi.org/10.1039/c8ay02422g, 2019.

Xia, F., Liu, Z., Zhao, M., Li, Q., Li, D., Cao, W., Zeng, C., Hu, Y., Chen, B., Bao, Q., Zhang, Y., He, Q., Lai, C., He, X., Ma, Z., Han, Y., and He, H.: High stability of autochthonous dissolved organic matter in karst aquatic ecosystems: Evidence from fluorescence, Water Res, 220, 118723, https://doi.org/10.1016/j.watres.2022.118723, 2022.

Yamashita, Y. and Jaffé, R.: Characterizing the interactions between trace metals and dissolved organic matter using excitation-emission matrix and parallel factor analysis, Environ Sci Technol, 42, 7374–7379, https://doi.org/10.1021/es801357h, 2008.

Zhou, Z., Liu, Z., and Guo, L.: Chemical evolution of Macondo crude oil during laboratory degradation as characterized by fluorescence EEMs and hydrocarbon composition, Mar Pollut Bull, 66, 164–175, https://doi.org/10.1016/j.marpolbul.2012.09.028, 2013.

LIST OF TABLES

Tab. 1

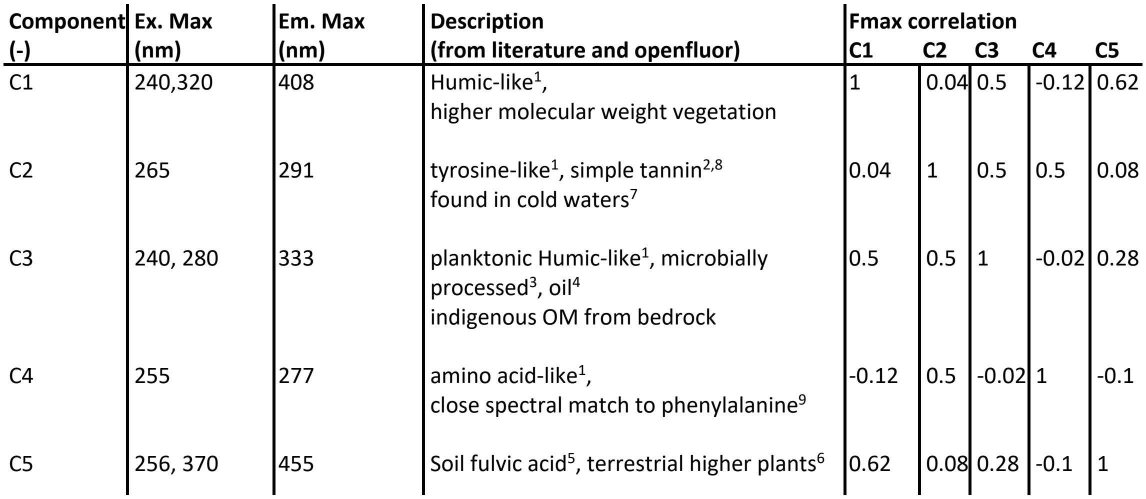

Component (-)	Ex. Max (nm)	Em. Max (nm)	Description (from literature and openfluor)	Fmax correlation				
				C1	C2	C3	C4	C5
C1	240,320	408	Humic-like[1], higher molecular weight vegetation	1	0.04	0.5	-0.12	0.62
C2	265	291	tyrosine-like[1], simple tannin[2,8] found in cold waters[7]	0.04	1	0.5	0.5	0.08
C3	240, 280	333	planktonic Humic-like[1], microbially processed[3], oil[4] indigenous OM from bedrock	0.5	0.5	1	-0.02	0.28
C4	255	277	amino acid-like[1], close spectral match to phenylalanine[9]	-0.12	0.5	-0.02	1	-0.1
C5	256, 370	455	Soil fulvic acid[5], terrestrial higher plants[6]	0.62	0.08	0.28	-0.1	1

Table 1:

PARAFAC model component properties. Ex_{max} and Em_{max} give wavelength of peak excitation-emission pairs (double peaks for humic-like components). Pearson correlation between individual components across all samples is given in the column Fmax correlation. EEM spectra are described from comparison to literature and the OpenFluor database. References from literature are [1]Coble et al., 2014 ; [2]Aitken et al., 2014, [3]Xia et al., 2022; [4]Zhou et al., 2013 ; [5]Yamashita and Jaffé, 2008 and [6]Cory and McKnight, 2005. Derived from OpenFluor are [7]Chen et al., 2018; [8]Dandrilli and McConnell, 2021 and [9]Wünsch et al., 2015.

Tab. 2

Location	**Cave Temp. (°C)**	**pCO$_2$ (ppm)**	**Cover thickness (m)**	**Drip rate (ml/min)**	**$\delta^{18}O$**	**Overall fluorescence (*R.U.*)**	**FI**	**Spectral slope**	**C3:(C1+C5) ratio**
(Abbr.)	*monthly mean (1SD)*	*Max (Min)*		*Mean (1SD)*	*variance*	*Mean (1SD)*	*Mean (1SD)*	*Mean (1SD)*	*Mean (1SD)*
Forest (FOR)	14.21 (0.56)	1496 (461)	14.47	0.35 (0.18)	0.477	47.4 (13.35)	1.66 (0.02)	1.14 (0.3)	0.25 (0.17)
Snowball (SNO)	14.21 (0.56)	1496 (461)	14.35	-	-	37.86 (12.15)	1.60 (0.03)	0.62 (0.21)	0.18 (0.14)
Gloria (GLO)	14.44 (0.27)	1582 (569)	8.72	0.22 (0.08)	0.09	22.56 (24.64)	1.65 (0.12)	0.99	0.76 (0.7)
Gravel (GRA)	13.9 (0.22)	2416 (509)	13.29	0.72 (0.38)	0.08	18.64 (19.32)	1.52 (0.16)	1.15	0.37 (0.25)
Skyscraper (SKY)	13.89 (0.17)	5390 (510)	27.62	89.22 (24.25)	0.05	26.76 (20.35)	1.72 (0.16)	0.83	0.47 (0.50)
Playground (PLA)	13.72 (0.16)	4199 (525)	29.45	1.22 (0.916)	0.04	20.34 (5.73)	1.73 (0.14)	-0.48	0.96 (0.57)
Mushroom (MUS)	13.6	-	23.21	-	-	10.87 (0.23)	1.55 (0.2)	0.91	0.22 (0.46)

Table 2:

Sampling locations discussed in this study, their overall cave properties and mean optical values. Variability is given in the form of one standard deviation (1 SD). Overall fluoresecence over the entire EEM is given in raman units (R.U.). FI is the fluorescence index (McKnight et al. 2001). Extended description of the overlying vegetation and cave setting can be found in the Supplementary Table 1.

LIST OF FIGURES

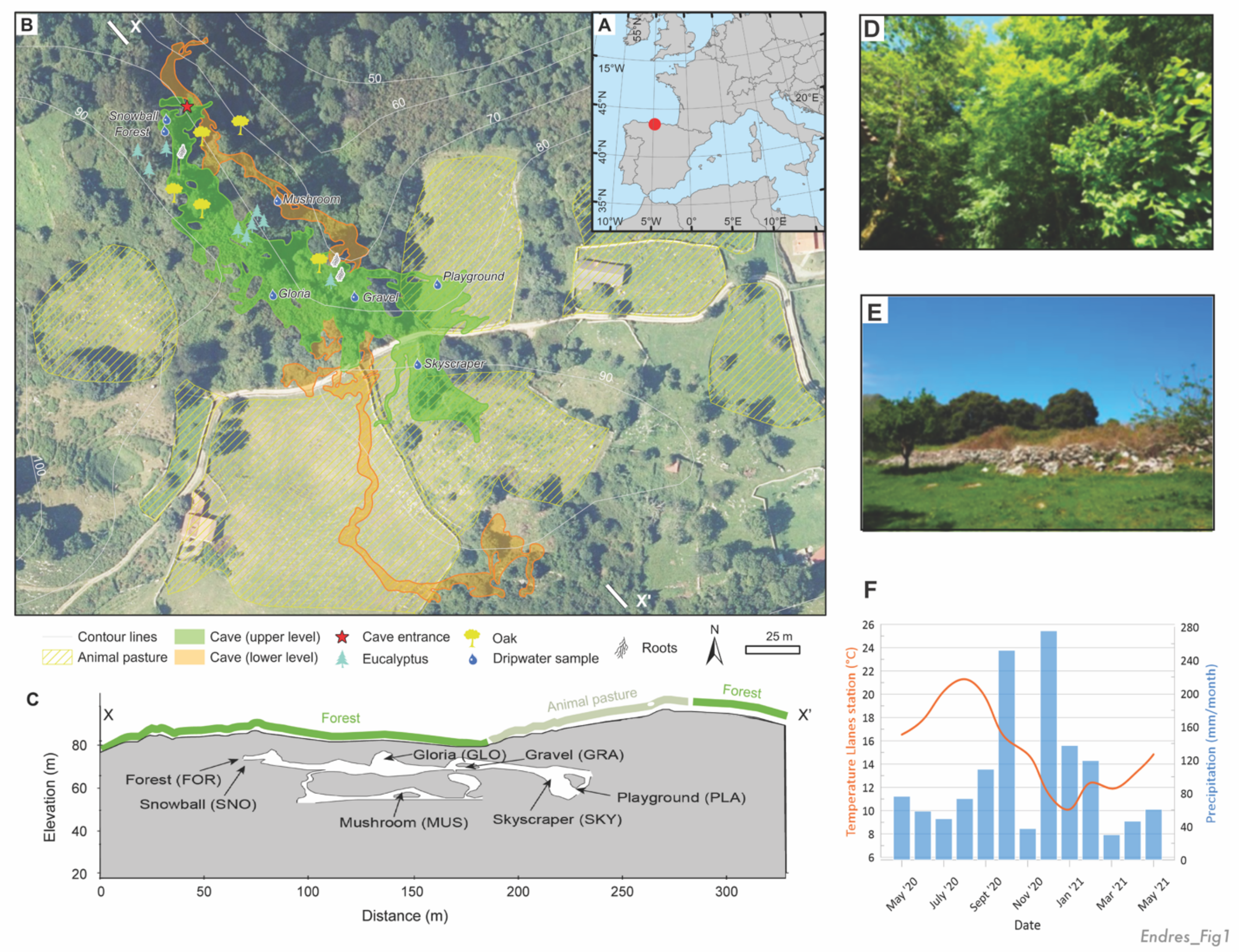

Figure 1.

Location, sampling map of locations in cave, and landcover and climatic setting. (A) Reference map with red circle denoting the cave location. (B) Plan map of the cave upper gallery (green outline) and lower gallery (orange outline) indicating the location of drip water sampling (labeled drop symbols) overlaid on aerial image from 2017 (Plan Nacional Ortofotografía Aérea - PNOA of Spanish IGN; available at https://centrodedescargas.cnig.es , last access: 30 December 2022), and showing topographic contours (white lines) with elevation above sea level (m). Pasture use and large trees are noted, as well as the position of root systems penetrating the cave. (C) Cross section (X to X') of cave with projected sampling locations. (D) Vegetation above sampling location FOR (May 2021), (E) Vegetation above

Sampling location PLA (May 2021). (F) Monthly mean air temperature and precipitation from Llanes weather station over sampling period (State Meteorological Agency of Spain, 2021).

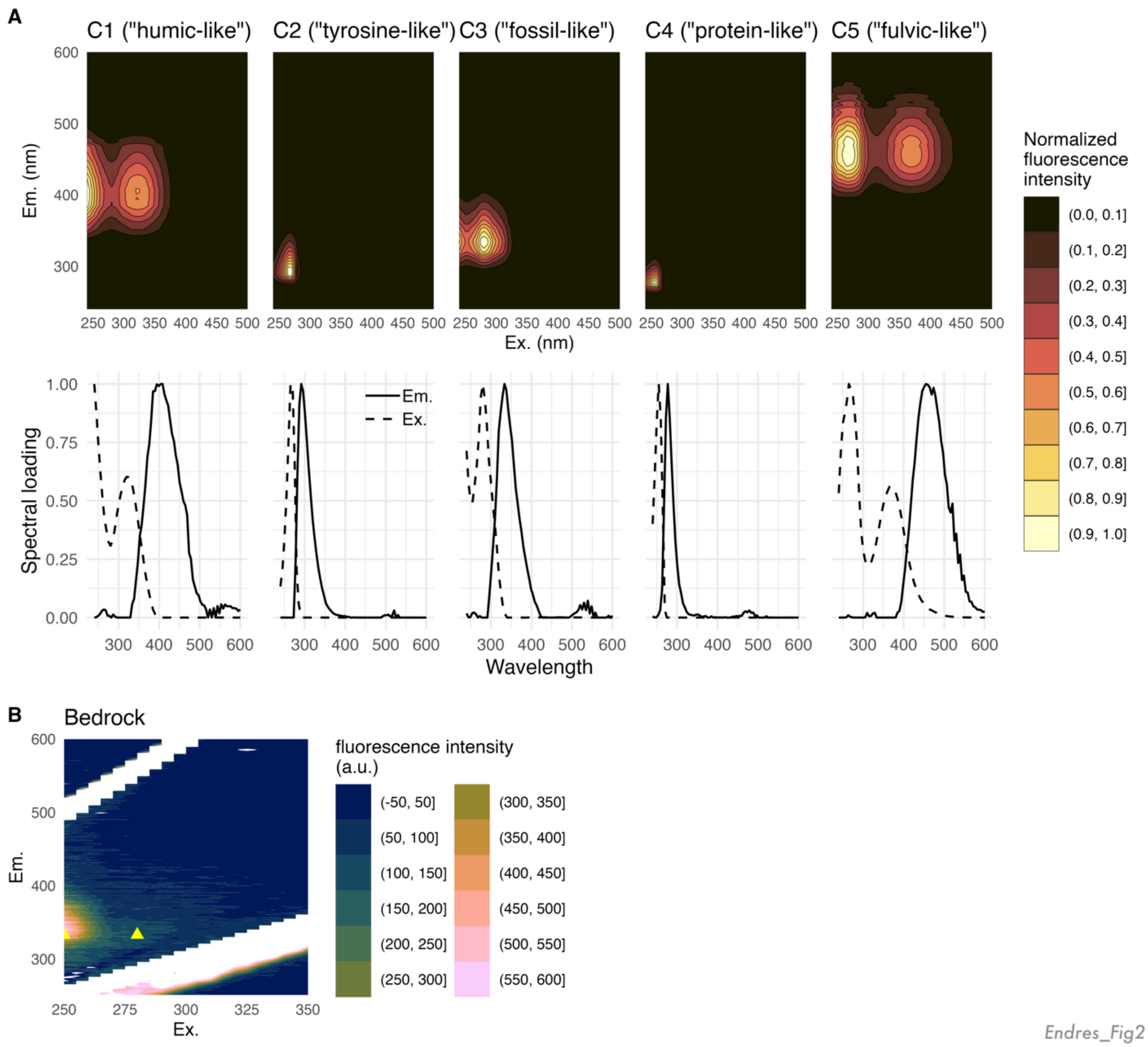

Endres_Fig2

Figure 2.

Dripwater components and bedrock endmember EEM. A) Drip water 5-component PARAFAC model and its spectral loadings. Fluorescence intensity is normalized to unity. Spectral loadings maxima in emission and excitation wavelengths are indicated with solid and dashed lines, respectively. B) EEM of dissolved organic-rich bedrock. Fluorescence intensity is given in arbitrary unit (a.u.). Yellow triangles indicate peak positions of drip water PARAFAC component C3 for comparison.

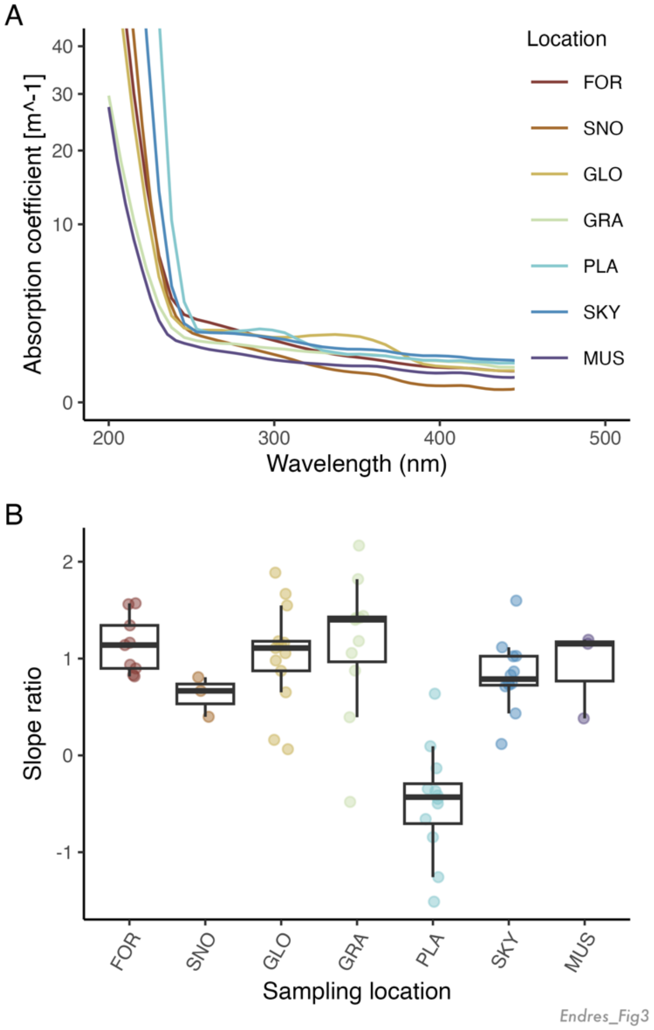

Figure 3.

Absorption properties of drip water samples grouped by location. A) Loess smoothed median absorption spectra for all locations. B) Spectral slope ratio values for individual absorbance measurements.

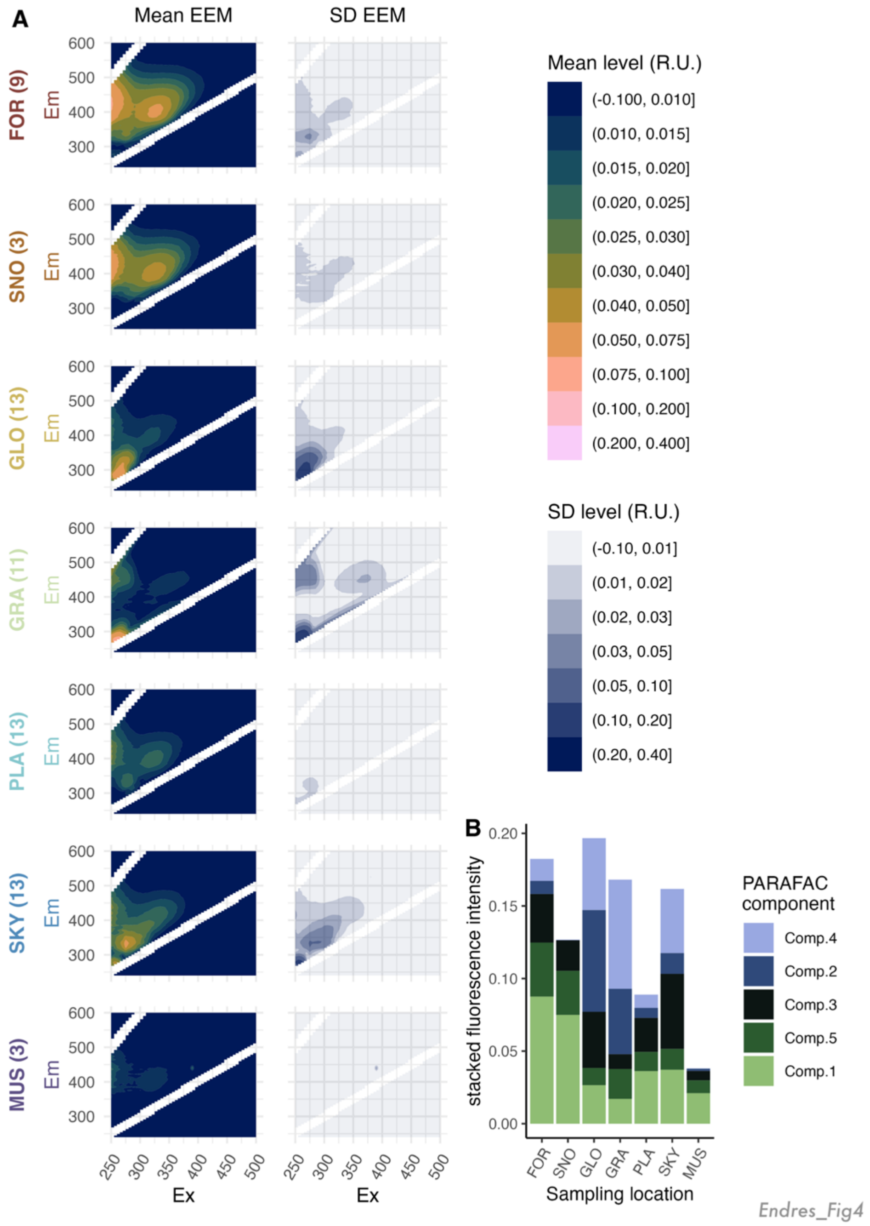

Figure 4.

A) Mean and standard deviation (SD) of Excitation-Emission Matrices (EEM) for each sampling location compiled over the monitoring period. Fluorescent intensities are given in Raman units (R.U.). B) mean intensity of all PARAFAC components for each sampling location, stacked to illustrate the total PARAFAC characterized fluorescence intensity at each location. Comp. 1 and Comp. 5 are described as “humic-like“ and “fulvic-like“, respectively. Comp. 3 is described as “fossil like”, Comp. 2 as “tyrosine-like”, and Comp. 4 as “protein like”.

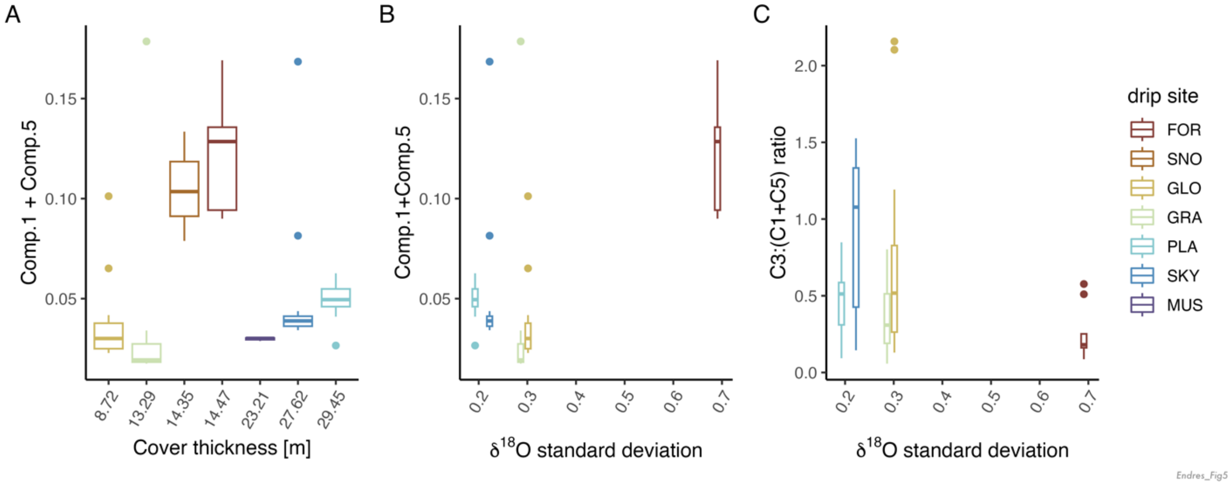

Figure 5.

Overview of the relationship between fluorescence and cave settings. A) comparison of the summed C1 and C5 (humic-like and fulvic-like) components plotted vs ascending thickness of bedrock cover over the drip sampling site. B) comparison of summed C1 and C5 components plotted vs the drip water δ^{18}O variance, which increases for shorter drip water residence times. C) comparison of the ratio of C3/(C1+C5) ratio of reworked or fossil components to humic-like and fulvic-like components, plotted vs the drip water δ^{18}O variance, which increases for shorter drip water residence times.

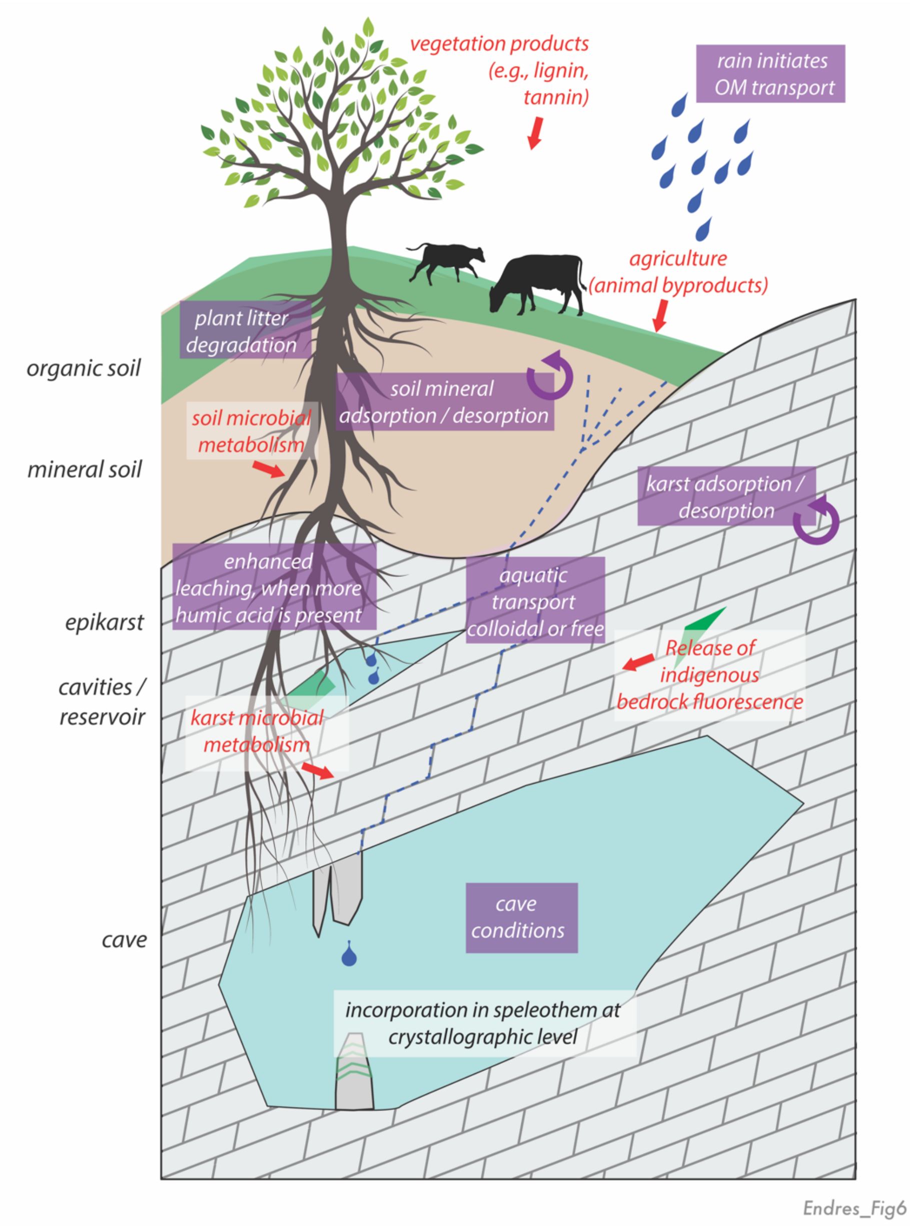

Figure 6.

Schematic of processes contributing to observed drip water fluorescence, from vegetation through soil, epikarst, and into cave. Red labels denote potential end member sources of different fluorescent organic component classes. Lavender boxes highlights proposed interactions between climate, vegetation/plant litter and bedrock including dissolution or leaching of bedrock by respired CO2, and adsorption of fluorescent matter to bedrock, as well as cave conditions potentially affecting incorporation of fluorescent organic matter in speleothems.

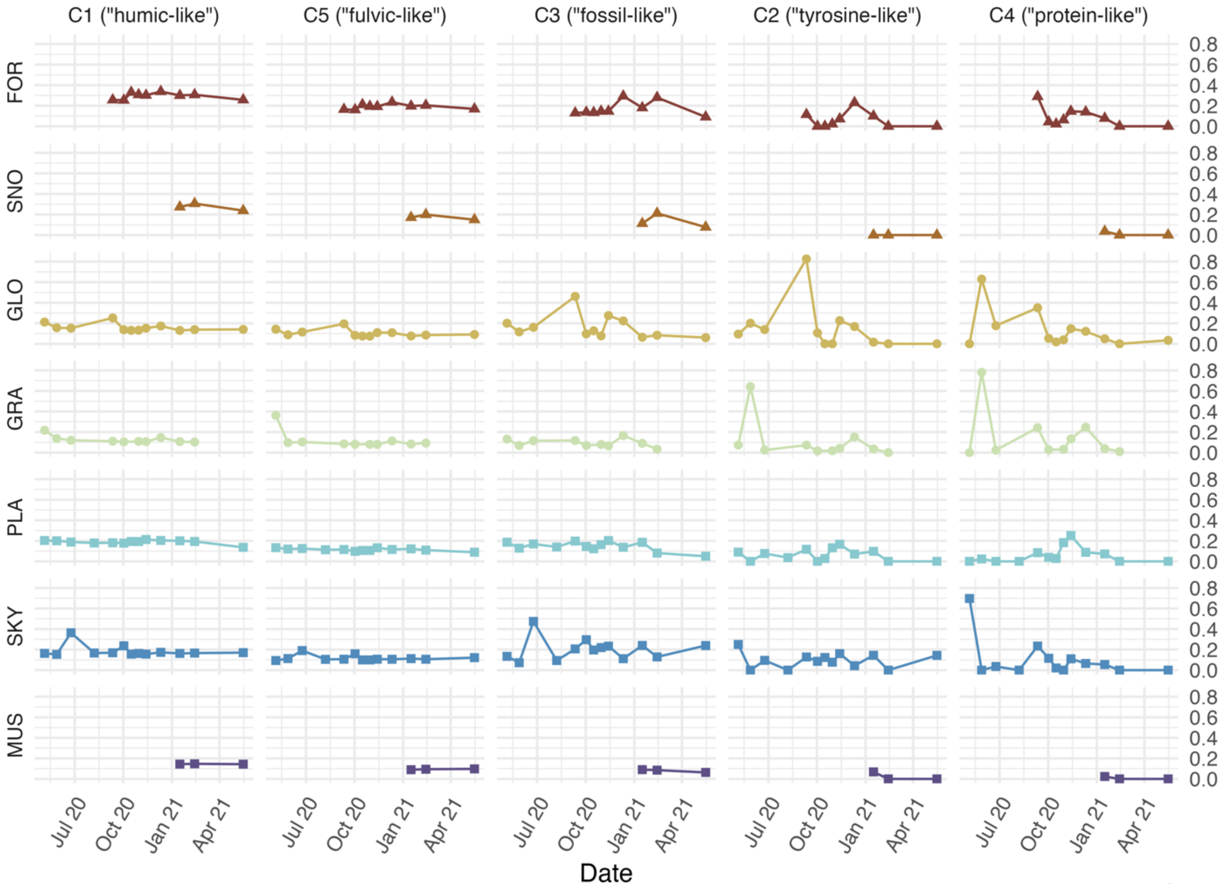

916

917 *Figure 7.*

918 Temporal evolution of the 5 components of the PARAFAC model throughout the monitored

919 period at each site. Each component y axis is given in normalized PARAFAC fluorescence intensity.

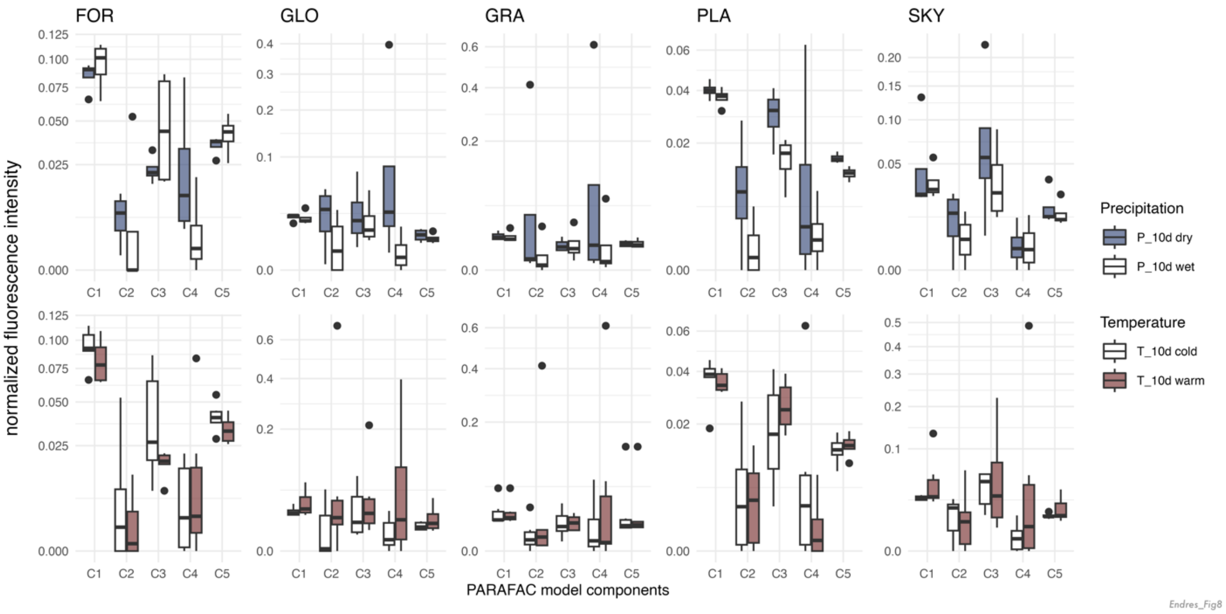

Figure 8.

Relationship of climate conditions 10 days prior to drip water sampling date versus fluorescence of each component for the five locations *FOR, GLO, GRA, PLA* and *SKY*. Upper row contrasts the fluorescence during four dates of dry weather in the 10 days prior to sampling, with fluorescence during four dates of wet weather in the 10 days prior to drip water sampling. The sample size of each group (n=4) was limited by total length of time series FOR. Lower row shows an analogous comparisons of groups during 4 dates of warm average surface air temperatures in the 10 days prior to drip water sampling vs 4 dates of cold average surface air temperatures in the 10 days prior to drip water sampling. The boxplot shows the median, first and third quartiles; the attached whisker extends from the hinges to the extreme value no further than 1.5x inter-quartile range and data outside of whisker is plotted as single points.

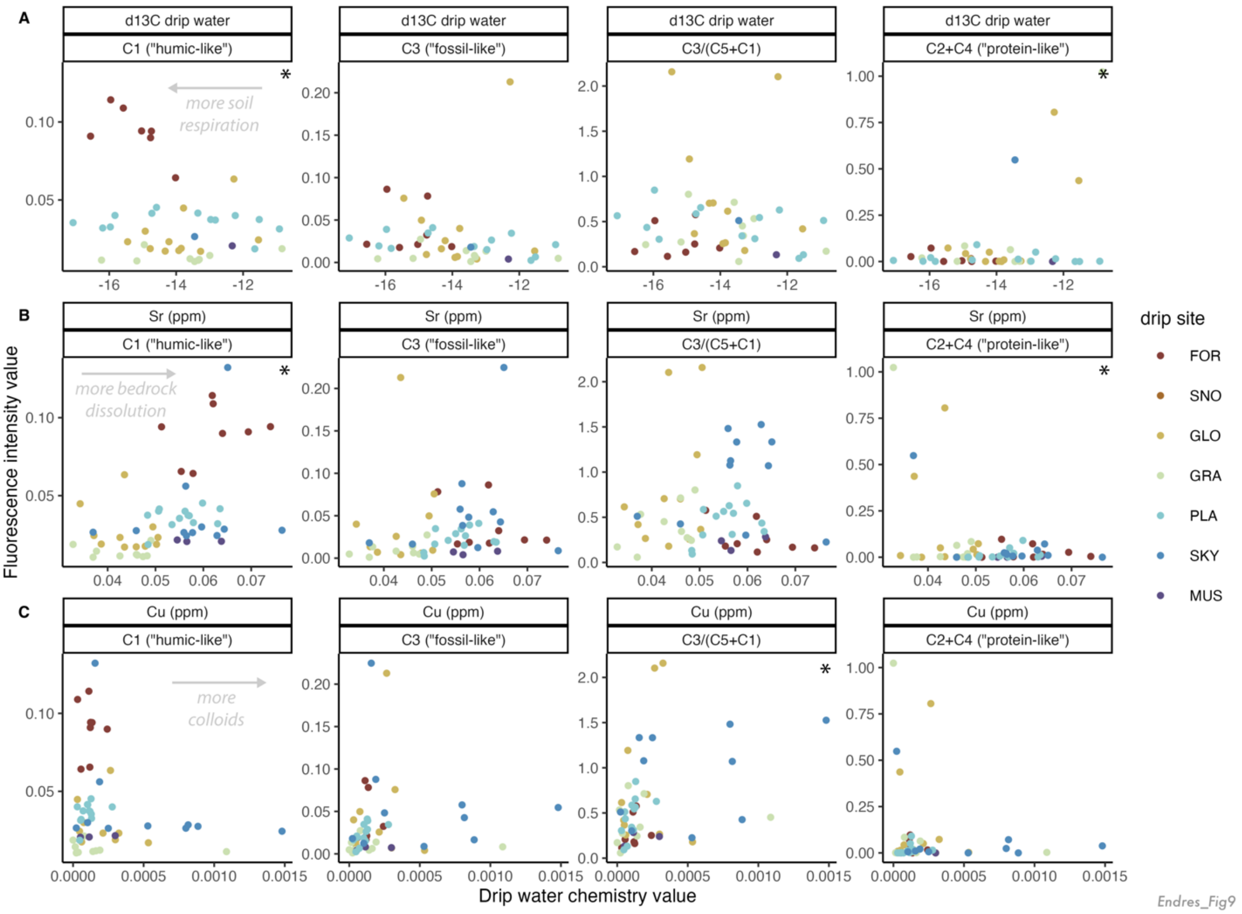

Figure 9.

Relationship between fluorescence parameters and indicators of the dissolution and karst conditions from drip water geochemistry. A) comparison of fluorescence components with the δ^{13}C of DIC in drip water, indicator of soil and epikarst CO_2 and respiration rates. B) comparison of fluorescence components with the drip water Sr concentration, an indicator of the extent of dissolution of karst bedrock. C) comparison of fluorescence components with the total drip water Cu concentration. Dripwater Cu is dominantly in the form of colloidal organic complexes.

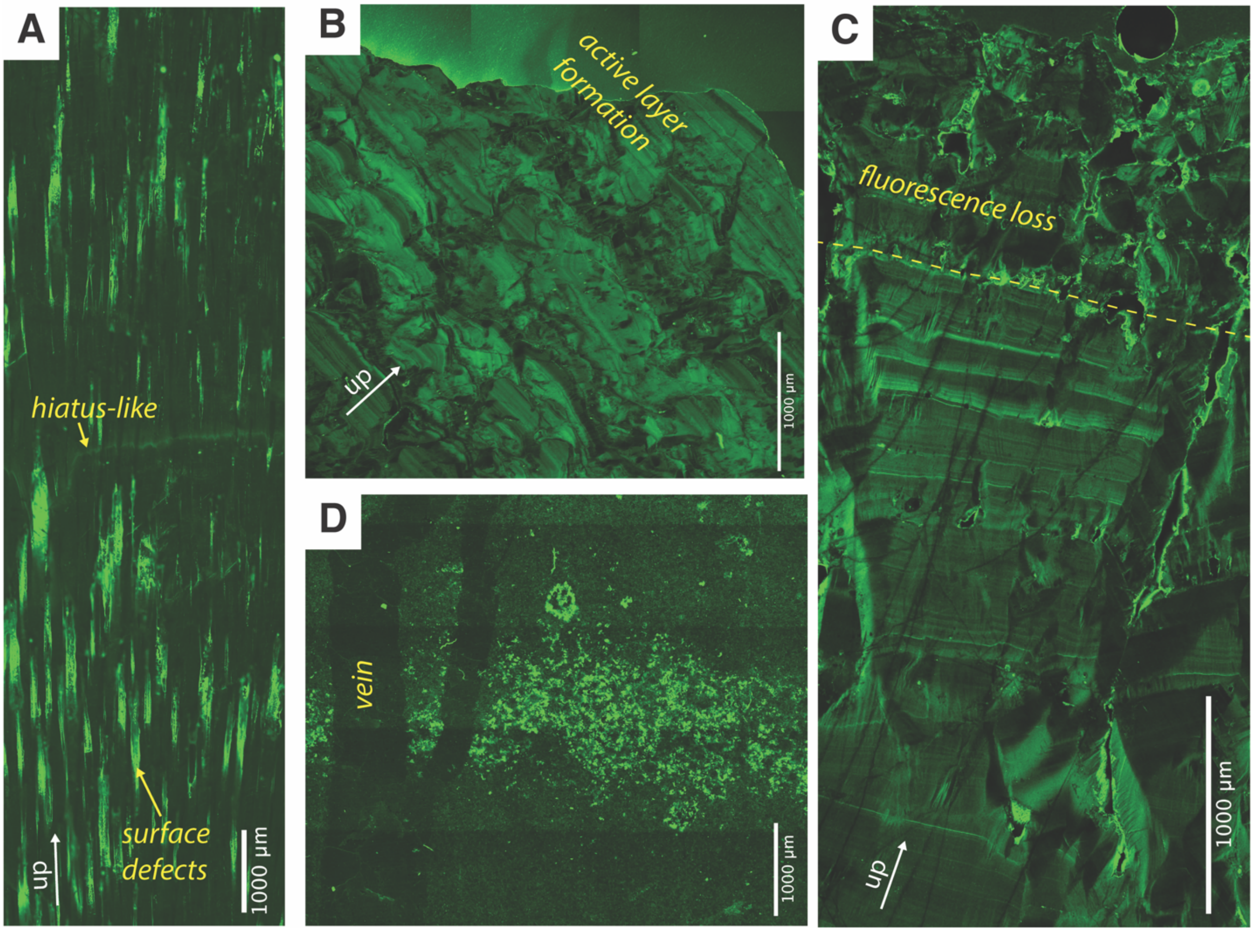

Figure 10.

Solid-phase fluorescence features of actively growing speleothems and bedrock from La Vallina Cave. A), stalagmite PG-2, sampled 5 m from drip water point PLA. B) stalagmite SKY, sampled beneath the drip water sample point SKY. C) stalagmite SNO, sampled beneath the drip water sample point SNO. D) polished bedrock. CLSM images were created with a Olympus Fluoview 3000 generated by Excitation at 488 nm and detection at 490-590 nm; images were and post-processed with Fiji (Schindelin et. al, 2012) and Adobe illustrator (Adobe Inc, 2019). Bomb spike age models for active stalagmites are presented in Sliwinski et al. (2022)

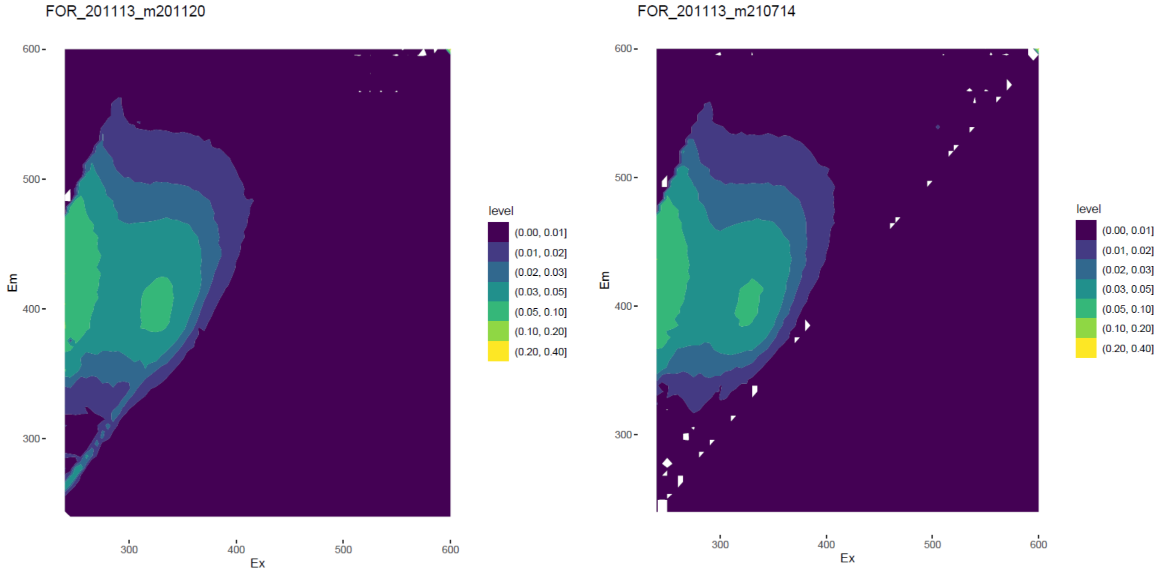

Supplementary Figure 1. Comparison of dripwater sample FOR collected 13 November 2020. Left image is EEM acquisition made on 20 November 2020, and the right image is acquisition on 14 July 2021.

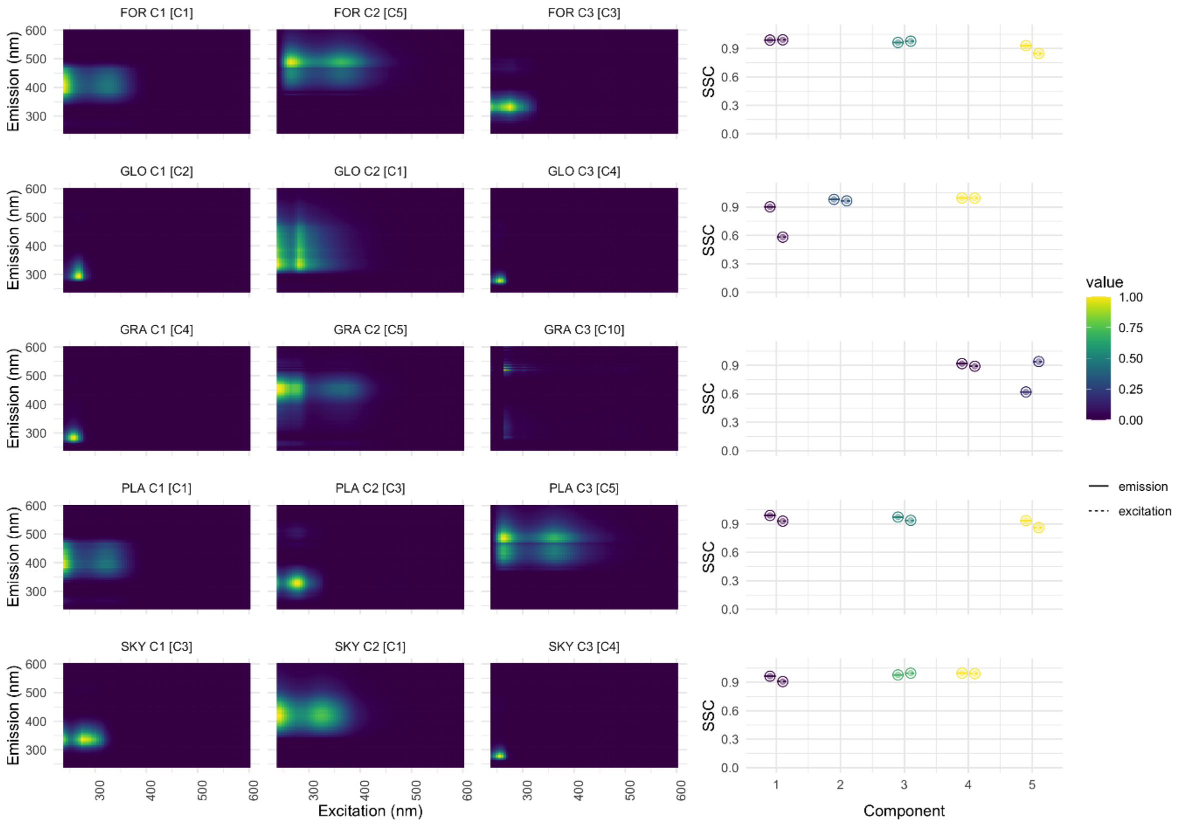

Supplementary Figure 2. Results from location-wise 3 component PARAFAC model reveal the presence of all five peaks as dominant features in single locations, but also across locations. Therefore, the 5-component model is able to represent the variability of the full dataset to a large degree. In detail: featuring high SSC values from 0.6-0.99, variability in location FOR is most similar to components C2,C5,C3; in GLO to C2,C1,C4; in GRA to C4,C5,(+Outlier); in PLA to C1,C3,C5 and in SKY to C3,C1,C4.

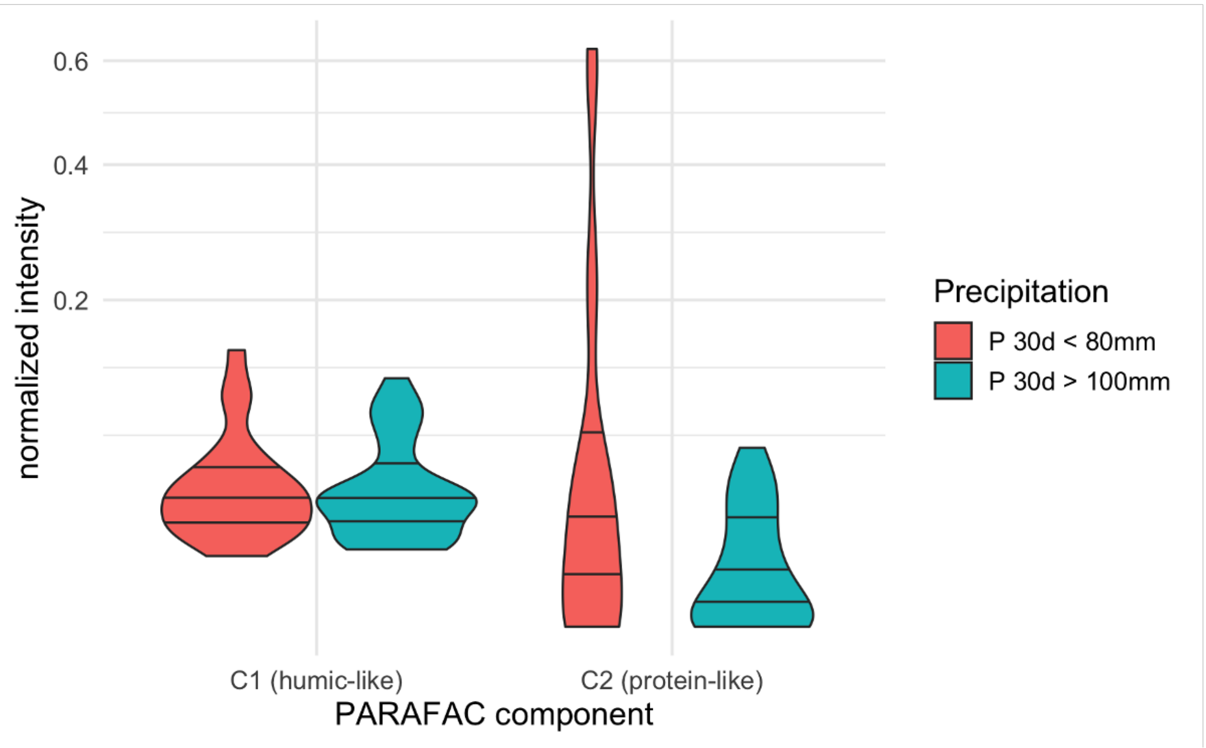

Supplementary Figure 3. Simplified to a humic-like and a protein-like component, the difference in intensity distribution in protein-like fluorescence between wet and dry conditions over the entire dataset is significant.

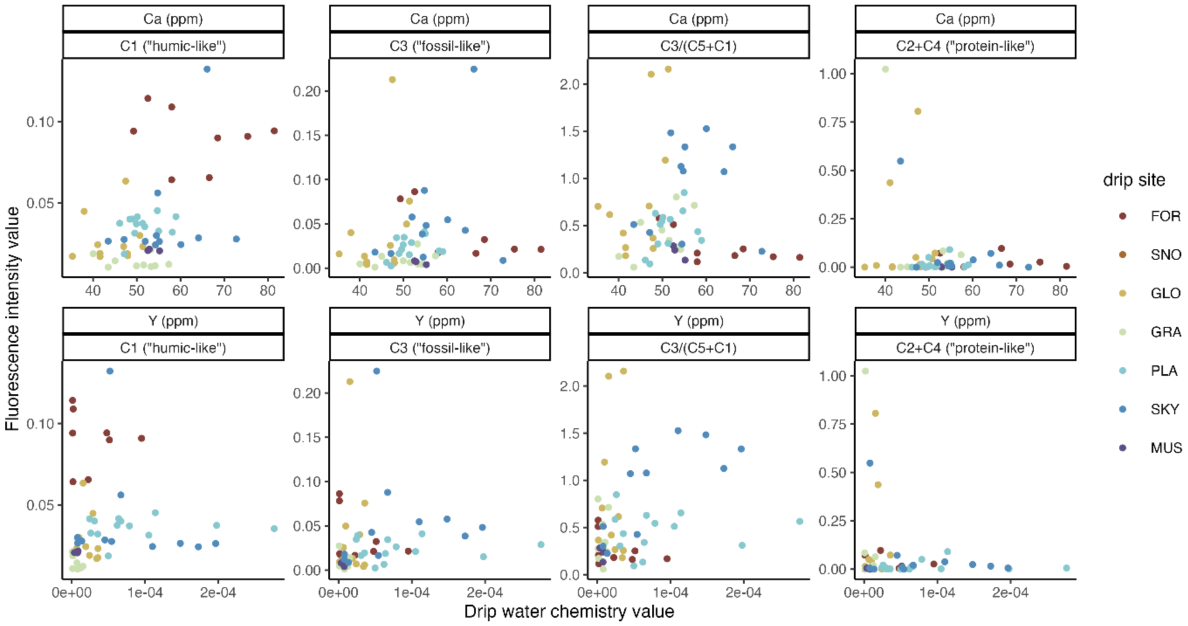

Supplementary Figure 4. Relationship between fluorescence parameters and indicators of the dissolution and karst conditions from dripwater geochemistry. Upper row, comparison of fluorescence components with dripwater Ca concentration, an indicator of the extent of dissolution of karst bedrock. Lower row, comparison of fluorescence components with the total dripwater Y concentration. Dripwater Y is dominantly in the form of colloidal organic complexes.

Supplementary Table 1. Description of vegetation and conditions above each drip location.

Location (Abbr.)	Vegetation and conditions above/at sampling location
Forest (FOR)	Oak, chestnut and large eucalyptus trees; also Fern, brambles and gorse. Roots of eucalyptus tree reach cave ceiling.
Snowball (SNO)	Oak, chestnut and large eucalyptus trees; also Fern, brambles and gorse. Roots of eucalyptus tree reach cave ceiling.
Gloria (GLO)	Vegetation is dominated by Bushes and Fern, two isolated trees (eucalyptus and oak) Doline is close by. Eucalyptus roots reach cave ceiling.
Gravel (GRA)	Vegetation is dominated by Bushes and Fern, two isolated trees (eucalyptus and oak) Doline is close by. Eucalyptus roots reach cave ceiling. cave ceiling filled with helictites and eccentric soda straws
Skyscraper (SKY)	Pasture, regularly used by cattle. Several sink holes are nearby.
Playground (PLA)	Pasture, regularly used by cattle. Several sink holes are nearby.
Mushroom (MUS)	Below hill slope, intermediate cover of some isolated trees and ferns.

Supplementary Equation 1

Beer's law:

$$\alpha(\lambda) = 2.303\ A(\lambda)/l$$

where $\alpha = absorption\ (m^{-1})$, A=Absorbance, l=cuvette pathlength (m) and $\lambda = wavelength\ (nm)$.